VALIDITY OF THE REYNOLDS EQUATION FOR MISCIBLE FLUIDS IN MICROCHANNELS

MATHIEU COLIN, THIERRY COLIN AND JULIEN DAMBRINE

MATHIEU COLIN AND THIERRY COLIN

Univ. Bordeaux, IMB, UMR 5251, F-33400 Talence, France,
CNRS, IMB, UMR 5251, F-33400 Talence, France.
INRIA, F-33400 Talence, France.

JULIEN DAMBRINE

LMA, Téléport 2- BP 30179
Boulevard Pierre et Marie Curie
86962 Futuroscope Chasseneuil Cedex, France

(Communicated by the associate editor name)

ABSTRACT. In this paper, we consider asymptotic models for miscible flows in microchannels. The characteristics of the flows in microfluidics imply that usually the Hele-Shaw approximation is valid. We present asymptotic models in the Hele-Shaw regime for flows of miscible fluids in a channel in the case where the bottom and the top of the channels have been modified in two different ways. The first case concerns a flat bottom with slip boundary conditions obtained by chemical patterning. The second one is a non-flat bottom with a non-slipping surface. We derive in both cases 2.5D and 2D asymptotic models. We prove global well-posedness of the 2D model. We also prove that both approaches are asymptotically equivalent in the Hele-Shaw regime and we present direct 3D simulations showing that for passive mixing strategy, the Hele-Shaw approximation is not valid anymore.

1. Introduction.

1.1. **Mixing in microchannels.** Microfluidics is a set of technics used to study complex fluids or biological fluids. It consists in performing experiments of fluids flows in webs of microchannels. Microchannels are typically 1 cm long and the section is roughly 100μm$\times100\mu$m. The velocity that are involved are typicaly less than 1cm.s^{-1}. Therefore the Reynolds numbers are small and the flows are laminar. In order to use microfluidics technics for chemistry, one has to be able to obtain fluid mixing. This is therefore an issue in this field.

The aim of this paper is to study asymptotic models and their validity for mixing in microchannels. Many approaches have been considered in order to enhance fluid mixing. Active mixing seems to be the most efficient approach but very difficult to handle for practical applications since one needs to build sophisticated devices. Devices for passive mixing are easier to obtain but the efficiency of such process is not clear. In this paper, we propose to investigate numerically some passive mixing strategies in the Hele-Shaw limit. We consider fluid flows that are driven only by the pressure gradient and no external constraint on the system are taken into account. Two kinds of mixing strategies are considered. Both involve modification of the surface of the top and the bottom of the microchannels. The first one uses a flat bottom channel with slip boundary conditions obtained from chemical patterning ([13], [14]); the second one uses a non-flat bottom channel with a non-slipping surface ([21], [22]). It is almost impossible to compare these mixing strategies by making direct 3D numerical computations. We propose here another approach relying on the Hele-Shaw approximation. It is an asymptotic process in which the flow is finally governed by the Reynolds equation (that is similar to Darcy's law for flows in porous media), see for example [1]. We show that, in this limit, it is possible to compare the efficiency of the mixing for both strategies: in this particular regime, they are equivalent in the sense that, given a non-flat bottom, one can find a patterning that leads to an equivalent asymptotic model. Nevertheless, we also present some numerical experiments proving that this result cannot be extrapolated to general flows in microchannels (that is, outside the range of validity of the Hele-Shaw approximation). More precisely, we show by a direct 3D computation that in the case of a non-flat bottom, the shapes of the Hele-Shaw solution and the 3D flow are very different and therefore, the asymptotic regimes are no longer valid. Note that we are not in the configuration where the Hele-Shaw approximation is used to study Saffman-Taylor fingering like in [18]. Indeed, in our case, the fluids are both injected at the inlet of the channel as shown on Figure (1).
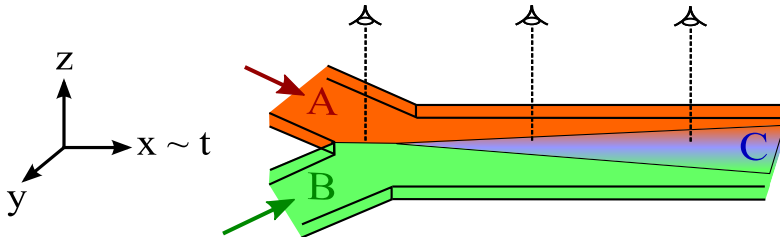
FIGURE 1. Example of a channel containing two fluids.

Moreover, the microfluidic flows considered in this paper are characterized by:
i) the jump of viscosity coefficient,
ii) the effect of confinement,
iii) the influence of the ratio of the flow-rates (pressure driven flows),
iv) the absence of gravity effects,
v) the effective mixing properties.
Therefore, some phenomena like instability due to gravity (see [7]) or shape interfaces and viscous fingering (see [15]) are not present in our case. Moreover, we are not concerned by lubricant effects due to roughness as studied in [4] where

the coupling between the size of the roughness and the thickness of the channel is investigated. One can see [9] for rigorous results concerning rough boundaries.

1.2. **The basic equations.** Usually, the flow dynamics in channels are governed by the Navier-Stokes equations. Nevertheless, the small dimensions involved in microfluidic applications lead to consider flows at low Reynolds numbers. As a consequence, the inertia terms in the Navier-Stokes model can be neglected in a first approximation. In this context, the velocity of the fluid is therefore given by the Stokes equations:

$$\begin{cases} \nabla \cdot [\eta \mathcal{D}(U)] = \nabla P, \\ \nabla \cdot U = 0, \end{cases} \tag{1.1}$$

where U denotes the velocity of the fluid flow, P the pressure, $\mathcal{D}(U)$ is the strain rate tensor given by $\mathcal{D}(U) = \dfrac{1}{2}\left(\nabla U + \nabla U^t\right)$.

In order to describe a mixing of two fluids, we introduce an order parameter φ (see for example [11]), which describes locally the volume fraction of each fluid in the mixture. It satisfies $\varphi \in [0, 1]$, $\varphi = 1$ in the fluid 1, $\varphi = 0$ in the fluid 2. Equipped with this parameter, it is possible to write a one fluid formulation for the mixing by using (1.1). The viscosity η is given as a function of η_1, η_2 (each fluid viscosity) and depends on φ. There are many different ways to describe $\eta(\varphi)$ (linear, cubic, tangential, non-monotonic [19]). In this paper we consider the linear approach: $\eta(\varphi) = \eta_1\varphi + \eta_2(1 - \varphi)$. The evolution of φ is given by a convection-diffusion equation:

$$\partial_t\varphi + U \cdot \nabla\varphi - \nabla \cdot [D(\varphi)\nabla\varphi] = 0, \tag{1.2}$$

where $D(\varphi)$ is the diffusion coefficient from one fluid into the other one.

In order to close the system given by (1.1) and (1.2), we need to introduce suitable boundary conditions. Let us first present the geometry of the channel we consider here:
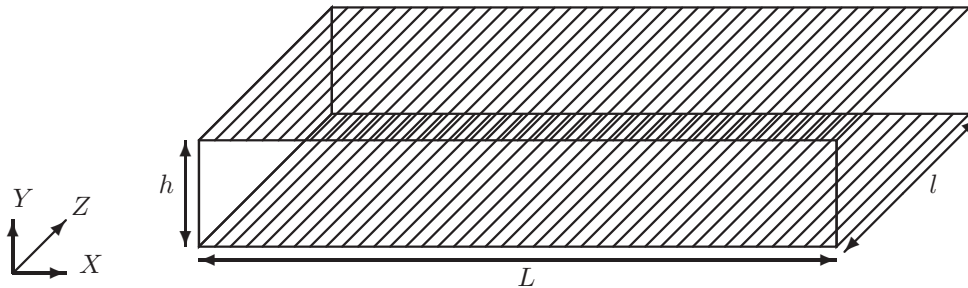
FIGURE 2. Schematic view of a microchannel and its characterisic dimensions.

h is the height of the channel, and for a non-constant height, we denote by $\bar{h}$ the maximum height and δh the amplitude of the variations. l denotes the width of the channel and L its length (see Figure 2). For the Stokes equations (1.1), we impose a Dirichlet boundary condition $U = U_0(y, z)$ at the inlet of the channel and $U = 0$ on the lateral walls; at the outlet we force the pressure to be $P = 0$. On the top and the bottom of the microchannel, we use various boundary conditions based upon the different approaches studied for mixing. We consider two types of channels. One is a flat bottom channel with slip boundary conditions and the other one is a non-flat bottom with a non-slipping surface (see Section 2 for a complete description). For

the convection-diffusion equation, we consider a Dirichlet boundary condition at the inlet $\varphi = \varphi_0(y, z)$ and $\dfrac{\partial \varphi}{\partial \nu} = 0$ everywhere else where ν denotes the outward normal of the domain.

One of our motivations is to introduce a reliable model in order to perform quick numerical simulations, using finite volume method. To this end, since the full 3D Stokes system is expensive in terms of computations, we present reduced models, based on the Hele-Shaw approximation. It consists in introducing two different scales in space by assuming that the variations in the vertical direction are much more rapid than that in the horizontal plane. Therefore, the integration of the Stokes equations (1.1) with respect to z (height) leads, after transformations, to a 2-D equation on the pressure P. The velocity is recovered by a Darcy law. The convection-diffusion Equation (1.2) is writing respectively in 3-D and 2-D providing two different models: the first one is called the 2.5 D model while the second one is a complete 2-D model. In this paper, the validity of the 2D system is discussed for various situations. We consider first viscous displacements involving simple geometry with no surface modification on the microchannel. The second case concerns different mixing strategies involving boundary conditions already studied in literature.

1.3. **Outline of the paper and main results.** In Section 2, we perform explicetly the Hele-Shaw approximation in the case of a flat channel with chemical patterning and in the case of a non-flat bottom. We first introduce 2.5D models. In both cases, the limit system is given as follows. The pressure $P(t, x, y)$ satisfies a 2D elliptic equation

$$\nabla_{xy} \cdot \left(K_j^{2D}(\varphi) \nabla_{xy} P(x, y) \right) = 0,$$

with $j = n$ or p (the index n stands for the case of a non-flat bottom while p stands for the case of a flat bottom with chemical patterning), see (2.25) or (2.33), where $K_n^{2D}(\varphi)$ or $K_p^{2D}(\varphi)$ are functions of (t, x, y) constructed from $\varphi(t, x, y)$ (see Section 2 for the formulas). From this pressure field, one first build the horizontal components $u(t, x, y, z)$ and $v(t, x, y, z)$ of the velocity by

$$\begin{pmatrix} u \\ v \end{pmatrix} = K_j^{3D}(\varphi) \nabla_{xy} P,$$

for $j = n, p$, see (2.26) or (2.34) where $K_j^{3D}(\varphi)$ are functions of (t, x, y, z). The vertical component of the velocity is recovered finally through the incompressibility condition by

$$w = - \int_0^z \nabla_{xy} \cdot \begin{pmatrix} u \\ v \end{pmatrix} (t, x, y, \sigma) d\sigma,$$

see (2.27) and (2.35).

In both cases, the order parameter φ solves the 3D convection-diffusion equation

$$\partial_t \varphi + \begin{pmatrix} u \\ v \\ w \end{pmatrix} \cdot \nabla_{xyz} \varphi - \nabla_{xyz} \left(D(\varphi) \nabla_{xyz} \varphi \right) = 0,$$

see (2.24) and (2.32). The model is said to be 2.5D since the velocity field and the order parameter φ are 3D but the velocity is derived from the pressure field $P(t, x, y)$ that solves a 2D equation. The 2D model is obtained at the end of Section 2 by investigating responses for which $\partial_z \varphi \sim 0$. One then obtains two different models, see Systems (2.37)-(2.39) and (2.40)-(2.42).

In Section 3, we propose some numerical computations. We first describe the numerical scheme that is used and then we perform some simulations in order to explain co-flow displacements and viscous fingering. Using the coefficients K_n^{2D} and K_p^{2D}, we show in what sense the two mixing strategies are equivalent and we explain how one can construct a patterning that leads to the same mixing than a given flat bottom in the Hele-Shaw regime. Then, in order to investigate the validity of the Hele-Shaw approximation, we compare numerically the 2.5D model with a full 3D computation in the case of a staggered herringbone micromixer. We show that, in this case, the Hele-Shaw approximation is not valid, therefore 3D computations are needed.

The appendix is devoted to the construction of a global, weak solution to the 2D model and to local in time strong solutions. The difficulty relies on the particular boundary conditions considered in this paper and for example, one has to prove that for any regular solution of the system, the velocity at the outlet of the channel is directed toward the exterior of the channel, which is not surprising from the physical point of view (see Lemma 5.2).

Notations: As usual, for a bounded domain Ω of $\mathbb{R}^d$, we denote by $L^p(\Omega)$ the Lebesgue space

$$L^p(\Omega) = \left\{ u \in \mathcal{S}^{'}(\Omega) \ / \ ||u||_p < +\infty \right\}$$

where

$$||u||_p = \left(\int_\Omega |u(x)|^p dx \right)^{\frac{1}{p}} \text{ if } 1 \le p < +\infty$$

and

$$||u||_\infty = \text{ess.sup} \left\{ |u(x)|; x \in \Omega \right\}.$$

We define the Sobolev space $H^m(\Omega)$ as follows

$$H^m(\Omega) = \left\{ u \in L^2(\Omega) \ / \ \forall \alpha \in \mathbb{N}^d, |\alpha| \le m, \partial^\alpha u \in L^2(\Omega) \right\}.$$

The corresponding norm is denoted $|| \cdot ||_{H^m}$. Let $\mathcal{X}$ be a Banach space. We denote by $L^p\left(0, T; \mathcal{X}\right)$ $(1 \le p \le +\infty)$ the space of functions $m \ : \ (0, T) \longrightarrow \mathcal{X}$ such that m is measurable and

$$\|m\|_{L^p\left(0,T;\mathcal{X}\right)} = \left(\int_0^T \|m(t)\|_\mathcal{X}^p dt \right)^{\frac{1}{p}} < +\infty \quad \text{if } 1 \le p < +\infty,$$

$$\|m\|_{L^\infty\left(0,T;\mathcal{X}\right)} = \sup_{t \in [0,T]} \|m(t)\|_\mathcal{X} < +\infty \quad \text{if } p = +\infty.$$

Different positive constants might be denoted by the same letter C.

2. **Obtention of the different models.** The Hele-Shaw approximation relies on the hypothesis that the characteristic vertical length is smaller than the horizontal ones. The aim of this section is to construct some models derived from this approximation starting from (1.1)-(1.2). Our strategy is somehow classical and we can refer to [11] for general theory of mixture as well as for the stability of an interface in a Hele-Shaw cell. Here the context is quite different: the gravity can be neglected and we are in a situation where the interface is stable. Our derivation of the models is classical, but we need the precise values of the coefficients and for the sake of completeness, we give the computations. In order to take into account that

the velocity variations in the vertical direction are very rapid compared to the horizontal ones, we introduce two different space scales, one for the vertical direction z and the other one for the horizontal variables (x, y). Recalling that a microfluidic channel is a simple rectangular domain, we assume that $h \ll \ell \ll L$ (see Figure 2). It is then natural to perform the change of variable

$$z \to \varepsilon z, \tag{2.3}$$

where ε is a small parameter describing the ratio between the height h and the others dimensions (L, ℓ) of the channel. We plug (2.3) into (1.1) and (1.2). The incompressibility condition (1.1) on the velocity $U = (u, v, w)$ gives

$$\partial_x u + \partial_y v + \frac{1}{\varepsilon} \partial_z w = 0. \tag{2.4}$$

Equation (2.4) implies that the third component of the velocity w has to be of order ε. We hence need to perform the following change of unknown:

$$w \to \varepsilon w. \tag{2.5}$$

Using (2.3) and (2.5) we can rewrite the Stokes equation (1.1). First, recall that the strain rate tensor $\mathcal{D}(U)$ is defined by

$$\mathcal{D}(U) = \frac{\nabla U + \nabla U^t}{2} = \frac{1}{2} \begin{pmatrix} 2\partial_x u & \partial_y u + \partial_x v & \partial_z u + \partial_x w \\ \partial_y u + \partial_x v & 2\partial_y v & \partial_z v + \partial_y w \\ \partial_z u + \partial_x w & \partial_z v + \partial_y w & 2\partial_z w \end{pmatrix}.$$

Hence, the stationary Stokes system (1.1) can be written as

$$\begin{cases} -\partial_x P + \partial_x(\eta(\varphi)2\partial_x)u + \partial_y(\eta(\varphi)(\partial_y u + \partial_x v)) + \partial_z(\eta(\varphi)(\partial_z u + \partial_x w)) = 0, \\ -\partial_y P + \partial_x(\eta(\varphi)(\partial_y u + \partial_x v)) + \partial_y(\eta(\varphi)2\partial_y v) + \partial_z(\eta(\varphi)(\partial_z v + \partial_y w)) = 0, \\ -\partial_z P + \partial_x(\eta(\varphi)(\partial_z u + \partial_x w)) + \partial_y(\eta(\varphi)(\partial_z v + \partial_y w)) + \partial_z(\eta(\varphi)2\partial_z w) = 0. \end{cases} \tag{2.6}$$

In view of (2.3) and (2.5), the system (2.6) becomes

$$\begin{cases} -\partial_x P + \partial_x(2\eta\partial_x u) + \partial_y(\eta\partial_y u) + \partial_y(\eta\partial_x v) + \frac{1}{\varepsilon^2}\partial_z(\eta\partial_z u) + \partial_z(\eta\partial_x w) = 0, & (2.7) \\ -\partial_y P + \partial_x(\eta\partial_y u) + \partial_x(\eta\partial_x v) + \partial_y(2\eta\partial_y v) + \frac{1}{\varepsilon^2}\partial_z(\eta\partial_z v) + \frac{1}{\varepsilon}\partial_z(\eta\partial_y w) = 0, & (2.8) \\ -\frac{1}{\varepsilon}\partial_z P + \frac{1}{\varepsilon}\partial_x(\eta\partial_z u) + \varepsilon\partial_x(\eta\partial_x w) + \frac{1}{\varepsilon}\partial_y(\eta\partial_z v) + \varepsilon\partial_y(\eta\partial_y w) + \frac{1}{\varepsilon}\partial_z(2\eta\partial_z w) = 0. & (2.9) \end{cases}$$

2.1. **The 2.5D equations.** At this step, we have no information on the order of magnitude of ∇P. Since $\varepsilon \ll 1$, in (2.7) and (2.8) the terms involving $\frac{1}{\varepsilon^2}$ are at least one order of magnitude bigger than the other ones. Since we consider pressure driven flows, we have to prescribe the balance between pressure and $\frac{1}{\varepsilon^2}$ terms in (2.7) - (2.8). For this purpose, one scales the pressure by

$$P \to \frac{1}{\varepsilon^2}P.$$

At first order (2.7), (2.8) and (2.9) give

$$\begin{cases} -\partial_x P + \partial_z(\eta\partial_z u) = 0, & (2.10) \\ -\partial_y P + \partial_z(\eta\partial_z v) = 0, & (2.11) \\ \partial_z P = 0. & (2.12) \end{cases}$$

Then Equations (2.10) and (2.11) can be rewritten as:

$$\partial_z \left[\eta \partial_z \begin{pmatrix} u \\ v \end{pmatrix} \right] = \nabla_{xy} P.$$

According to (2.12), P is independent of z. Then, integrating along the z direction, we get:

$$\partial_z \begin{pmatrix} u \\ v \end{pmatrix} = \nabla_{xy} P \left(\frac{z}{\eta} + \frac{A(x,y)}{\eta} \right), \tag{2.13}$$

where A is a scalar function of (x,y) generated by the integration along z. In the general case, η depends on the local composition $\varphi(t,x,y,z)$ of the mixing and Equation (2.13) becomes

$$\partial_z \begin{pmatrix} u \\ v \end{pmatrix} = \nabla_{xy} P \left(\frac{z}{\eta(\varphi)} + \frac{A(x,y)}{\eta(\varphi)} \right). \tag{2.14}$$

Integrating again Equation (2.14) along the z direction, we obtain

$$\begin{pmatrix} u \\ v \end{pmatrix} (t,x,y,z) = \nabla_{xy} P \left(\int_0^z \frac{\sigma}{\eta(\varphi)} d\sigma + A(x,y) \int_0^z \frac{1}{\eta(\varphi)} d\sigma + B(x,y) \right), \tag{2.15}$$

where B is a function of (x,y) generated by the integration along z. Equation (2.15) can be understood as a Darcy law. As already mentioned, in this paper, for practical applications, we consider two different cases. The first one deals with a non-flat bottom with no-slip boundary conditions. The second one deals with a flat bottom with a chemical patterning of the surface inducing slip for the flow. We now derive the complete system in both cases.

• Non-flat bottom with no-slip boundary conditions. In this case, the boundary conditions for the velocity read

$$\begin{pmatrix} u \\ v \\ w \end{pmatrix} (x,y,0) = \begin{pmatrix} u \\ v \\ w \end{pmatrix} (x,y,h) = 0. \tag{2.16}$$

This provides $B(x,y) = 0$, by taking $z = 0$ in Equation (2.15). Taking now $z = h$, we obtain

$$A(x,y) = - \frac{\displaystyle\int_0^h \frac{\sigma}{\eta(\varphi)} d\sigma}{\displaystyle\int_0^h \frac{1}{\eta(\varphi)} d\sigma}. \tag{2.17}$$

Denoting by

$$K_n^{3D}(\varphi) = \int_0^z \frac{\sigma}{\eta(\varphi)} d\sigma - \frac{\displaystyle\int_0^h \frac{\sigma}{\eta(\varphi)} d\sigma}{\displaystyle\int_0^h \frac{1}{\eta(\varphi)} d\sigma} \int_0^z \frac{1}{\eta(\varphi)} d\sigma, \tag{2.18}$$

we rewrite Equation (2.15) as

$$\begin{pmatrix} u \\ v \end{pmatrix} (x,y,z) = K_n^{3D}(\varphi) \nabla_{xy} P. \tag{2.19}$$

Rewriting the incompressibility condition (1.1), and taking (2.15) into account, we obtain

$$\partial_z w = -\nabla_{xy} \cdot \begin{pmatrix} u \\ v \end{pmatrix},$$

$$= -\nabla_{xy} \cdot \left(K_n^{3D}(\varphi) \nabla_{xy} P \right). \tag{2.20}$$

By integrating (2.20) from 0 to h we get

$$\int_0^h \nabla_{xy} \cdot \left(K_n^{3D}(\varphi(x,y,\sigma)) \nabla_{xy} P(x,y) \right) d\sigma = 0,$$

which provides denoting by

$$K_n^{2D}(\varphi) = \int_0^h K_n^{3D}(\varphi(x,y,\sigma)) d\sigma, \tag{2.21}$$

the following equation on P

$$\nabla_{xy} \cdot \left(K_n^{2D}(\varphi) \nabla_{x,y} P(x,y) \right) = 0. \tag{2.22}$$

The vertical velocity $w(x,y,z)$ is recovered by integrating (2.20) from 0 to z

$$w(x,y,z) = -\int_0^z \nabla_{xy} \cdot \begin{pmatrix} u \\ v \end{pmatrix} (x,y,\sigma) d\sigma. \tag{2.23}$$

By performing the change of variables (2.3) in the 3D convection-diffusion Equation (1.2), one gets:

$$\partial_t \varphi + \begin{pmatrix} u \\ v \\ w \end{pmatrix} \cdot \nabla \varphi - \nabla_{x,y} \cdot (D(\varphi) \nabla_{x,y} \varphi) - \frac{1}{\varepsilon^2} \partial_z (D(\varphi) \partial_z \varphi) = 0.$$

The complete model then reads

$$\begin{cases} \partial_t \varphi + \begin{pmatrix} u \\ v \\ w \end{pmatrix} \cdot \nabla \varphi - \nabla_{x,y} \cdot (D(\varphi) \nabla_{x,y} \varphi) - \frac{1}{\varepsilon^2} \partial_z (D(\varphi) \partial_z \varphi) = 0, & (2.24) \\[2mm] \nabla_{xy} \cdot \left(K_n^{2D}(\varphi) \nabla_{x,y} P(x,y) \right) = 0, & (2.25) \\[2mm] \begin{pmatrix} u \\ v \end{pmatrix} = K_n^{3D}(\varphi) \nabla_{xy} P, & (2.26) \\[2mm] w = -\int_0^z \nabla_{xy} \cdot \begin{pmatrix} u \\ v \end{pmatrix} (x,y,\sigma) d\sigma. & (2.27) \end{cases}$$

• <u>Slip patterned flat channel</u>. We consider the case of a flat channel with a chemical patterning on the top and the bottom. The classical slip condition reads $\frac{\partial U_\tau}{\partial \vec{n}} = -\frac{1}{\overline{L}} U_\tau$, where U_τ represents the tangential velocity, and $\overline{L}$ a characteristic length for the slip phenomenon. In our case, we define the top and bottom slip length patterns $L_t(x,y)$ and $L_b(x,y)$. The tangential velocity at the top and the bottom of a flat channel is the velocity along the (x,y) direction and the normal derivative is the derivative along the z direction. The slip conditions are:

$$\begin{aligned} \partial_z \begin{pmatrix} u \\ v \end{pmatrix} (x,y,0) &= -\frac{1}{L_b(x,y,\varphi(0))} \begin{pmatrix} u \\ v \end{pmatrix} (x,y,0), \\ \partial_z \begin{pmatrix} u \\ v \end{pmatrix} (x,y,h) &= \frac{1}{L_t(x,y,\varphi(h))} \begin{pmatrix} u \\ v \end{pmatrix} (x,y,h). \end{aligned} \tag{2.28}$$

Taking respectively $z = 0$ and $z = h$ in Equation (2.14) and (2.15), we have

$$\frac{A(x,y)}{\eta(\varphi(x,y,0))} = -\frac{B(x,y)}{L_b(x,y)}, \tag{2.29}$$

$$A(x,y)\left(\frac{1}{\eta(\varphi(x,y,h))} - \frac{1}{L_t(x,y)}\int_0^h \frac{1}{\eta(\varphi(x,y,\sigma))}\mathrm{d}\sigma\right) - \frac{B(x,y)}{L_t(x,y)}$$

$$= \frac{1}{L_t(x,y)}\int_0^h \frac{\sigma}{\eta(\varphi(x,y,\sigma))}\mathrm{d}\sigma - \frac{h}{\eta(\varphi(x,y,h))}. \tag{2.30}$$

From (2.29) and (2.30), one obtains

$$A(x,y) = \frac{\displaystyle\int_0^h \frac{\sigma}{\eta(\varphi(x,y,\sigma))}\mathrm{d}\sigma - \frac{hL_t(x,y)}{\eta(\varphi(x,y,h))}}{\left(\dfrac{L_t(x,y)}{\eta(\varphi(x,y,h))} + \dfrac{L_b(x,y)}{\eta(\varphi(x,y,0))}\right) - \displaystyle\int_0^h \frac{1}{\eta(\varphi(x,y,\sigma))}\mathrm{d}\sigma}, \tag{2.31}$$

$$B(x,y) = -L_b(x,y)\frac{A(x,y)}{\eta(\varphi(0))}.$$

Introducing

$$K_p^{2D}(\phi) = \int_0^h \left(\int_0^z \frac{\sigma}{\eta(\varphi)}\mathrm{d}\sigma + A(x,y)\int_0^z \frac{1}{\eta(\varphi)}\mathrm{d}\sigma + B(x,y)\right)\mathrm{d}z,$$

$$K_p^{3D}(\phi) = \int_0^z \frac{\sigma}{\eta(\varphi)}\mathrm{d}\sigma + A(x,y)\int_0^z \frac{1}{\eta(\varphi)}\mathrm{d}\sigma + B(x,y),$$

the complete model reads

$$\begin{cases} \partial_t\varphi + \begin{pmatrix} u \\ v \\ w \end{pmatrix} \cdot \nabla\varphi - \nabla_{x,y}\cdot(D(\varphi)\nabla_{x,y}\varphi) - \frac{1}{\varepsilon^2}\partial_z(D(\varphi)\partial_z\varphi) = 0, & (2.32) \\[2ex] \nabla_{xy}\cdot\left(K_p^{2D}(\varphi)\nabla_{x,y}P(x,y)\right) = 0, & (2.33) \\[2ex] \begin{pmatrix} u \\ v \end{pmatrix} = K_p^{3D}(\varphi)\nabla_{xy}P, & (2.34) \\[2ex] w = -\int_0^z \nabla_{xy}\cdot\begin{pmatrix} u \\ v \end{pmatrix}(x,y,\sigma)d\sigma. & (2.35) \end{cases}$$

2.2. **Simplified 2D models.** In this section, we introduced 2D simplified models as follows. As $\varepsilon \to 0$, Equation (2.32) leads to $\partial_z\varphi = 0$ at the first order, and therefore, φ is independent of z. Averaging (2.32) over $[0,h]$ and using $\partial_z\varphi = 0$ at $z = 0$ and $z = h$ gives

$$\partial_t\varphi + \begin{pmatrix} \overline{u} \\ \overline{v} \end{pmatrix} \cdot \nabla\varphi - \nabla_{x,y}\cdot(D(\varphi)\nabla_{x,y}\varphi) = 0,$$

where

$$\begin{pmatrix} \overline{u} \\ \overline{v} \end{pmatrix} = \frac{1}{h}\int_0^h \begin{pmatrix} u \\ v \end{pmatrix}(t,x,y,z)dz.$$

We now explain how one can compute this averaged velocity in both cases.

● 2D model for non-flat bottom. Since φ is independent of z, we obtain from (2.17)

$$A(x,y) = -\frac{h(x,y)}{2},$$
$$B(x,y) = 0. \tag{2.36}$$

In this case, we need to compute $\begin{pmatrix} \overline{u} \\ \overline{v} \end{pmatrix} = \overline{K}_n^{3D}(x,y)\nabla_{x,y}P$. Using (2.36) in (2.18) and (2.21), one gets:

$$K_n^{2D}(x,y) = -\frac{h^3(x,y)}{12\eta(\varphi)},$$
$$\overline{K}_n^{3D}(x,y) = -\frac{h^2(x,y)}{12\eta(\varphi)}.$$

From (2.24)-(2.27), we get the following 2D model

$$\begin{cases} \nabla_{xy} \cdot \left[K_n^{2D}(x,y)\nabla_{xy}P \right] = 0, & (2.37) \\[2mm] \begin{pmatrix} \overline{u} \\ \overline{v} \end{pmatrix}(x,y) = \overline{K}_n^{3D}(x,y)\nabla_{xy}P, & (2.38) \\[2mm] \partial_t\varphi + \begin{pmatrix} \overline{u} \\ \overline{v} \end{pmatrix} \cdot \nabla_{x,y}\varphi - \nabla_{x,y} \cdot (D(\varphi)\nabla_{x,y}\varphi) = 0. & (2.39) \end{cases}$$

● 2D model for a slip patterned flat channel. Let us rewrite (2.31) assuming that $\overline{\varphi}$ and therefore η is independent of z

$$A(x,y) = \frac{h}{2}\left(\frac{h - 2L_t(x,y)}{L_t(x,y) + L_b(x,y) - h} \right),$$
$$B(x,y) = -\frac{L_b(x,y)}{\eta(\varphi)}A(x,y).$$

In the same way as above, we obtain

$$K_p^{2D}(x,y) = \frac{1}{\eta}\left(\frac{h^3}{6} - \frac{h^2}{4}\left(\frac{h^2 - 2h(L_b(x,y) + L_t(x,y)) + 4L_b(x,y)L_t(x,y)}{h - L_t(x,y) - L_b(x,y)} \right) \right),$$
$$\overline{K}_p^{3D}(x,y) = \frac{1}{\eta}\left(\frac{h^2}{6} - \frac{h}{4}\left(\frac{h^2 - 2h(L_b(x,y) + L_t(x,y)) + 4L_b(x,y)L_t(x,y)}{h - L_t(x,y) - L_b(x,y)} \right) \right),$$

which leads to the following model

$$\begin{cases} \nabla_{xy} \cdot \left[K_p^{2D}(x,y)\nabla_{xy}P \right] = 0, & (2.40) \\[2mm] \begin{pmatrix} \overline{u} \\ \overline{v} \end{pmatrix}(x,y) = \overline{K}_p^{3D}(x,y)\nabla_{xy}P, & (2.41) \\[2mm] \partial_t\varphi + \begin{pmatrix} \overline{u} \\ \overline{v} \end{pmatrix} \cdot \nabla_{x,y}\varphi - \nabla_{x,y} \cdot (D(\varphi)\nabla_{x,y}\varphi) = 0. & (2.42) \end{cases}$$

Remark 1. *In addition, if we choose the same slip length patterns on the top and bottom of the channel (i.e. $L_t = L_b = \overline{L}$) we get much simpler expressions for the permeability coefficients $K_p^{2D}(x,y)$ and $\overline{K}_p^{3D}(x,y)$:*

$$K_p^{2D}(x,y) = \frac{1}{\eta}\left(\frac{h^3}{6} - \frac{h^2}{4}\left(h - 2\overline{L}(x,y) \right) \right),$$
$$\overline{K}_p^{3D}(x,y) = \frac{1}{\eta}\left(\frac{h^2}{6} - \frac{h}{4}\left(h - 2\overline{L}(x,y) \right) \right).$$

Of course we recover in this case the formulas given in [8] *for example.*

3. **Numerical methods.** The aim of this section is to present an efficient numerical scheme in 2D and 3D for the different systems introduced in Section 2. First recall the general form of the system we deal with

$$
\begin{cases}
\nabla \cdot [K(X, \varphi(t, X)) \nabla P(t, X)] = 0, & (3.43) \\
U(t, X) = F(\varphi(t, X), \nabla P(t, X)), & (3.44) \\
\partial_t \varphi(t, X) + U(t, X) \cdot \nabla \varphi(t, X) - \nabla \cdot (D(\varphi(t, X)) \nabla \varphi(t, X)) = 0. & (3.45)
\end{cases}
$$

Here U represents the fluid velocity, this quantity being respectively 2D as in Section 2.2, $U = (\overline{u}, \overline{v})$ or 3D as in Section 2.1, $U = (u, v, w)$. X represents the space variable ((x, y) in 2D or (x, y, z) in 3D). In the Darcy law (3.44), the function F depends on the model we consider and more particularly on the geometry of the channel (slip patterns or non flat bottom). We use a very simple discretization of the problem that we present rapidly below.

3.1. **Semi-discretization in time.** Introducing $t_n = n\Delta t$, we denote $\varphi^n = \varphi(t_n, X)$, $U^n = U(t_n, X)$, $P^n = P(t_n, X)$. Since Equations (3.43) and (3.44) are stationary, their time discretizations are straightforward and reads

$$
\begin{cases}
\nabla \cdot [K(X, \varphi^n \nabla P^n] = 0, \\
U^n(X) = F(P^n, \varphi^n).
\end{cases}
$$

In Equation (3.45), we use a classical finite difference scheme

$$
\partial_t \varphi(X, t_{n+1/2}) \sim \frac{\varphi^{n+1} - \varphi^n}{\Delta t}.
$$

The transport part is treated by an explicit scheme while a semi-implicit θ-scheme is used for the diffusion part:

$$
\frac{\varphi^{n+1} - \varphi^n}{\Delta t} + U^n \cdot \nabla \varphi^n - \nabla \cdot (D(\varphi^n) \nabla (\theta \varphi^n + (1-\theta) \varphi^{n+1}) = 0.
$$

Then, the semi-discretized system in time can be rewritten as:

$$
\begin{cases}
\nabla \cdot [K(X, \varphi^n) \nabla P^n] = 0, & (3.46) \\
U^n = F(P^n, \varphi^n), & (3.47) \\
[1 - \Delta t (1 - \theta) (\nabla \cdot (D(\varphi^n) \nabla)] \varphi^{n+1} = \varphi^n - \Delta t (U^n \cdot \nabla \varphi^n + \theta \nabla \cdot (D(\varphi^n) \nabla \varphi^n)) & (3.48)
\end{cases}
$$

3.2. **Space discretization.** In this section, we consider a regular cartesian mesh, which is well-adapted when one deals with microfluidic flows, $x_i = i\Delta x$, $y_j = j\Delta y$ in 2D and $z_k = k\Delta z$ in 3D, where $i = 1, ..., N_x$, $j = 1, ..., N_y$, $k = 1, ..., N_z$. N_x, N_y, N_z represent the mesh resolution. In general, for any variable V, we denote: $V(t_n, x_i, y_j, z_k) = V_{i,j,k}^n$ and we use a staggered grid. More precisely, the velocity nodes are placed in the following way (see Figure 3)

$$
\begin{aligned}
u_{i,j,k} &= u(x_{i-\frac{1}{2}}, y_j, z_k), \\
v_{i,j,k} &= v(x_i, y_{j-\frac{1}{2}}, z_k), \\
w_{i,j,k} &= w(x_i, y_j, z_k),
\end{aligned}
$$

whereas the pressure is computed on the nodes of the mesh $P_{i,j,k} = P(x_i, y_j, z_k)$.
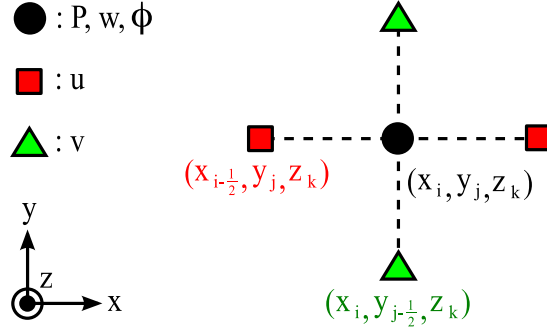
FIGURE 3. Placement of the unknowns on the staggered grid.

We now present briefly the essential point of our spatial discretization. We choose a finite volume formulation. The unit cell is given by

$$\Omega_{ijk} = [x_{i-\frac{1}{2}}, x_{i+\frac{1}{2}}] \times [y_{i-\frac{1}{2}}, y_{i+\frac{1}{2}}] \times [z_{i-\frac{1}{2}}, z_{i+\frac{1}{2}}].$$

The equation (3.48) include a transport term $U^n \cdot \nabla$ which is approached with a Weighted Essentially Non-Oscillatory scheme (WENO 5) which reduces numerical diffusion for smooth enough solutions. This transport scheme is stable under the CFL condition (see [16]):

$$\Delta t < \frac{1}{\dfrac{||u||_\infty}{\Delta x} + \dfrac{||v||_\infty}{\Delta y} + \dfrac{||w||_\infty}{\Delta z}}.$$

We still have to give the discretization of the elliptic parts of System (3.46)-(3.48), which can be written in the following form

$$\alpha S - \nabla \cdot \left(K \nabla S \right) = f,$$

where $S = P$, $\alpha = 0$, $K = K_n^{2D}(\varphi^n)$ and $f = 0$ in (3.46) and $S = \varphi^{n+1}$, $\alpha = 1$, $K = \delta t \mathcal{D}(\varphi^n)$ and $f = \varphi^n - \delta t V^n \cdot \nabla \varphi^n$ in (3.48). Recall that the finite volume methods consists in computing the circulation of $K(x,y)\nabla_{xy}P \cdot \vec{n}$ around each unit cell Ω_{ijk} of the mesh, we obtain from Equation (3.46), denoting Γ_{ijk} the boundary of Ω_{ijk}

$$\int_{\Omega_{ijk}} \nabla \cdot \left(K_n^{2D}(\varphi)\nabla P \right) = \int_{\Gamma_{ijk}} K_n^{2D}(\varphi)\nabla P \cdot \vec{n} \qquad (3.49)$$

Pointing out that both P and φ are calculated in the middle of each unit cell, ∇P is naturally evaluated on each part of Γ_{ijk} while the coefficient $K_n^{2D}(\varphi)$ is computed by interpolation. We propose here to use the harmonic mean value on each lattices of the boundary, keeping in mind that this process conserves the flux continuity. Then introducing:

$$K_{i-\frac{1}{2},j,k} = \frac{2K_{i,j,k}K_{i-1,j,k}}{K_{i,j,k} + K_{i-1,j,k}}, K_{i+\frac{1}{2},j,k} = \frac{2K_{i,j,k}K_{i+1,j,k}}{K_{i,j,k} + K_{i+1,j,k}}$$

$$K_{i,j-\frac{1}{2},k} = \frac{2K_{i,j,k}K_{i,j-1,k}}{K_{i,j,k} + K_{i,j-1,k}}, K_{i,j+\frac{1}{2},k} = \frac{2K_{i,j,k}K_{i,j+1,k}}{K_{i,j,k} + K_{i,j+1,k}},$$

$$K_{i,j,k-\frac{1}{2}} = \frac{2K_{i,j,k}K_{i,j,k-1}}{K_{i,j,k} + K_{i,j,k-1}}, K_{i,j,k+\frac{1}{2}} = \frac{2K_{i,j,k}K_{i,j,k+1}}{K_{i,j,k} + K_{i,j,k+1}},$$

we then obtain from (3.49):

$$\int_{\Omega_{ijk}} \nabla \cdot (K_{i,j} \nabla P_{i,j}) \sim \frac{\Delta y \Delta z}{\Delta x}(P_{i+1,j,k} - P_{i,j,k})K_{i+\frac{1}{2},j,k} - \frac{\Delta y \Delta z}{\Delta x}(P_{i,j,k} - P_{i-1,j,k})K_{i-\frac{1}{2},j,k}$$

$$+ \frac{\Delta x \Delta z}{\Delta y}(P_{i,j+1,k} - P_{i,j,k})K_{i,j+\frac{1}{2},k} - \frac{\Delta x \Delta z}{\Delta y}(P_{i,j,k} - P_{i,j-1,k})K_{i,j-\frac{1}{2},k}$$

$$+ \frac{\Delta x \Delta y}{\Delta z}(P_{i,j,k+1} - P_{i,j,k})K_{i,j,k+\frac{1}{2}} - \frac{\Delta x \Delta y}{\Delta z}(P_{i,j,k} - P_{i,j,k-1})K_{i,j,k-\frac{1}{2}}.$$

The same procedure is applied on Equation (3.48). The discretization of the other terms is classical and we refer to [5] for more details.

3.3. **Viscous effects.** The aim of this section is to investigate the validity of the models introduced in Section 2 with two classical test case dealing with viscous effects: the interface displacement and the viscous fingering.

3.3.1. *Co-flow displacements.* The firts test case concerns the mixing of two fluids injected in a Y-shaped microchannel (Figure 4). Since we consider only the horizontal displacements, we choose the 2D model (2.37)-(2.39) equipped with a linear viscosity law. We consider a flat geometry, that is $h(x, y)$ is constant, and a no-slip condition at the top and the bottom of the channel. The diffusion coefficient is also supposed to be constant.
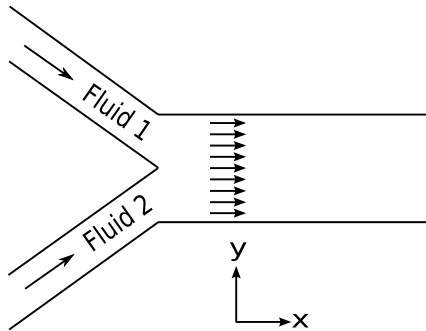
FIGURE 4. Schematic view of the experimental setup for the study of two fluids interdiffusion.

It is usually accepted that the displacement of the interface is influenced by the viscosity contrast defined in the following way

$$\lambda = \frac{\eta_1 - \eta_2}{min(\eta_1, \eta_2)}. \tag{3.50}$$

Of course, since one deals with miscible fluids, it is not easy to characterize the position of the interface since the notion of interface is not clear by itself! For that reason, in order to measure the interface displacement along the cross section direction we use a first order moment including the first order derivative with respect to y of the local composition parameter φ

$$M_1(x, t) = \int_{-D}^{D} y \partial_y \varphi(x, y, t) dy.$$

In the following simulations, we expect the most viscous fluid (the one with the biggest hydraulic resistance) to be pushed by the less viscous fluid in the cross direction of the channel. We also expect that the walls have an influence on this displacement.

For a low viscosity contrasts ($\lambda \ll 1$) this influence should be neglectible, and hence the interface displacement M_1 should depend linearly on λ. On the other hand, if we choose a larger viscosity contrast, the walls effects should be the most important ($\dfrac{\partial M_1}{\partial \lambda} \ll 1$). From the physical point of view, one can say that at the end of the channel, where the viscous displacement process is over, the flow-rates in each fluid are equal, *i.e.*

$$u_1 l_1 = u_2 l_2, \tag{3.51}$$

where u_1 and u_2 are the horizontal components of the velocity in the fluids 1 and 2. l_1 and l_2 represent the width occupied by the fluid 1 and 2 in the channel. These lengths can be expressed as a function of the displacement of the interface M_1: $l_1 = l/2 + M_1$ and $l_2 = l/2 - M_1$ (see Fig 5).
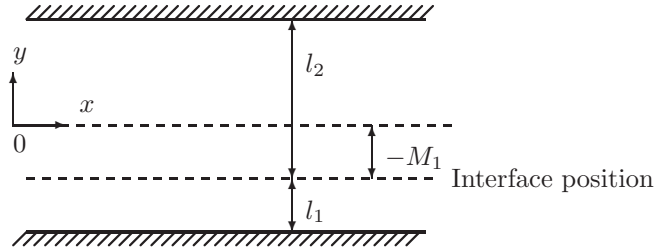
FIGURE 5. Representation of the different lengths l_1, l_2, M_1 involved in the study of the displacement of the interface (thick dashed line).

Thanks to the Darcy law (2.15), we have

$$\begin{aligned}
u_1 &= -\partial_x P \frac{h^2}{12\eta_1}, \\
u_2 &= -\partial_x P \frac{h^2}{12\eta_2}.
\end{aligned} \tag{3.52}$$

Using (3.51) and (3.52) we get

$$-\partial_x P \frac{h^2}{12\eta_1} l_1 = -\partial_x P \frac{h^2}{12\eta_2} l_2.$$

At the end of the displacement process, $\partial_x P$ is the same in each fluid. We hence have

$$\frac{l_1}{\eta_1} = \frac{l_2}{\eta_2}. \tag{3.53}$$

Using the expressions of l_1 and l_2 and (3.53) we finally obtain

$$\frac{M_1}{l} = \frac{\eta_2 - \eta_1}{2(\eta_2 + \eta_1)}. \tag{3.54}$$

Setting $f(\eta_1, \eta_2) = \dfrac{\eta_2 - \eta_1}{2(\eta_2 + \eta_1)}$, and according to (3.54), the relative displacement $\dfrac{M_1}{l}$ of a fluid due to a viscous effect should be predicted by $\dfrac{M_1}{l} = f(\eta_1, \eta_2)$. This assertion is checked in the following numerical simulations.

We use this particular channel geometry: length $L = 1300\mu m$, width $W = 200\mu m$. The characteristics of the two fluids are: same entry velocity $\overline{U_0} = 1.8 * 10^{-2} m.s^{-1}$, same density $\rho = 1.2 * 10^3 kg.m^{-3}$, we also keep the viscosity of the fluid two constant $\eta_2 = 0.67 Pa.s$ (glycerol viscosity). The other fluid viscosity vary from $\eta_1 = 8.375.10^{-2} Pa.s$ to $\eta_1 = 5.36 Pa.s$ (i.e $\varepsilon \in [-4, 4]$).

Before presenting our simulations, we ensure the discretization error to be small enough for the comparisons we wish to do. In order to find the mesh resolution which would fit this criteria, we need to perform a convergence calculus. Therefore, we compare the results given on the quantity $M_1(L, t)$ by simulations with the physical conditions described above, for different mesh resolutions (Figure 6).
The convergence on M_1 is rather quick. This is due to the fact that M_1, which only gives an information on the position of the middle of the interface, is not affected by any numerical diffusion. As we can see on Figure 6, an eligible resolution in this case would be $100 * 80$.
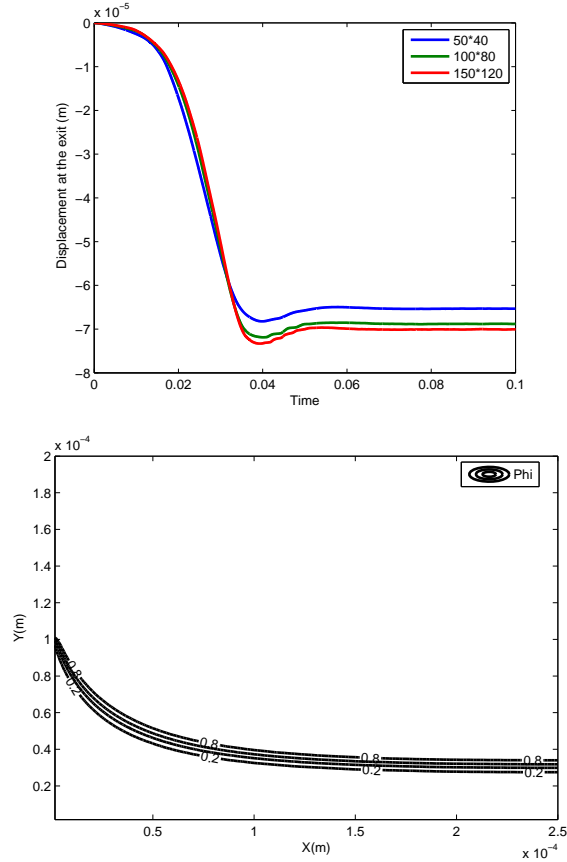
FIGURE 6. Left: Numerical convergence on the displacement M_1 as a function of time. Right: example of a map on the mixing composition $\varphi(x, y)$ in the channel.

As we can see on Figure 7 (left), as the contrast λ between the viscosities η_1 and η_2 increases, the position of the interface $M_1(X, T)$ gets closer to the borders. As foreseen, if the viscosity contrast is big enough ($\lambda \gg 1$), the displacement tends to be independent of λ. Moreover, a linear behavior on M_1 for little viscosity contrasts seems to appear. It means that for little displacements, the interface is not influenced by presence of the walls. It seems that this behavior tends to disappear when $\lambda > 1$ (*i.e.* viscosity variations greater than 100%).
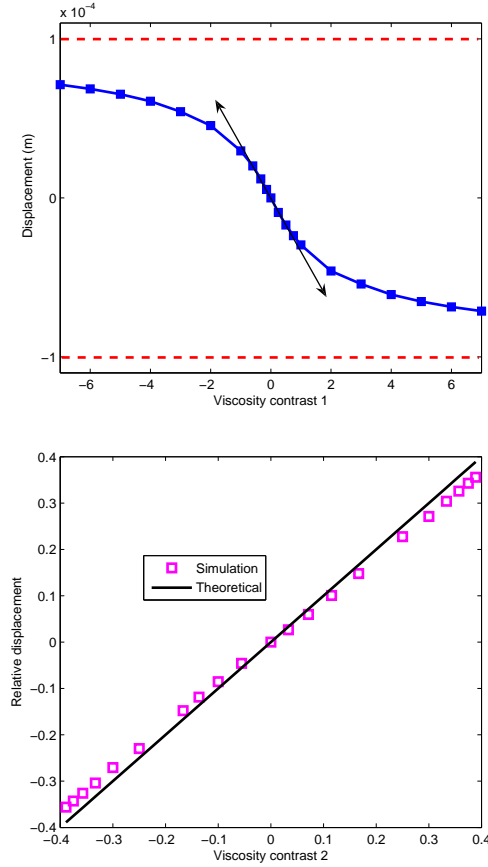
FIGURE 7. Left: displacement M_1 of the interface in the channel as a function of the viscosity contrast λ. Right: relative displacement $\dfrac{M_1}{l}$ of the interface in the channel as a function of $f(\eta_1, \eta_2)$.

We can see on Figure 7 (right) that simulations for different values of $f(\eta_1, \eta_2)$ (squares) nicely fits the theoretical displacement as described in (3.54) (black line) which validates the model in this case. Differences seem to occur as $|f(\eta_1, \eta_2)|$ grows. It can be related to the wall effect that can be noticed on Figure 6 (left) for $t \sim 0.4$.

All these results can hence lead us to think that the model used here works well for the co-flow interdiffusion case, see [6] for comparison with the experiments.

3.3.2. *Viscous fingering.* In this section we study an other example of viscous displacement that involves the z direction: the viscous fingering. The experiment is the following (see Figure 8): a fluid 1 with a viscosity η_1 is injected in a channel containing a fluid 2 with a viscosity η_2. In this study, we are interested in the profile of the interface in the $(\vec{x}, \vec{z})$ plane. The flow along the z direction is a Poiseuille flow which tends to form finger shaped interfaces influenced by the viscosities η_1 and η_2.
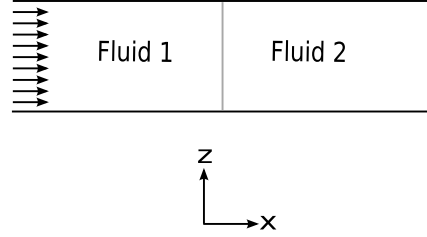
FIGURE 8. Schematic view of the experimental setup for the study of the viscous fingering

The suitable 2.5D model fitted to this experiment is composed by Equations (2.24)-(2.27) with a flat geometry and no-slip boundary conditions. The channel geometry chosen here is $L = 2000\mu m$, $W = 200\mu m$, $h = 80\mu m$. The profiles shown in Figure 9 correspond to two different viscosity gaps ($\eta_1 > \eta_2$ and $\eta_1 < \eta_2$). Those profiles seem to be physically relevant, however, further validation from the experimental point of view is needed in this case that can be done using advanced imaging techniques such as confocal microscopy, as shown in [10].
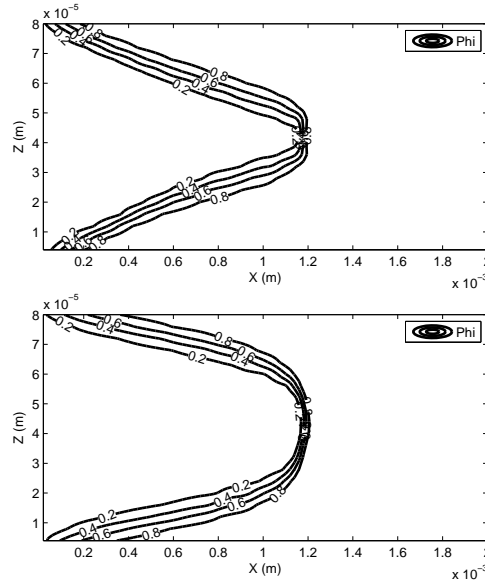
FIGURE 9. Map of $\varphi(x, y, t = 0.06s)$, left: $\eta_1 = 2$, $\eta_2 = 0.67$, right: $\eta_1 = 0.67$, $\eta_2 = 2$; initially filled with fluid 1

3.4. Classical passive mixing strategies involving both boundary conditions.

3.4.1. *Equivalence of the two models.* In this section, we investigate the influence of the boundary conditions in the process of mixing fluids. We consider two types of

boundary conditions: the slip ones and the no-slip ones. For simplicity, we assume that the viscosity η is constant and we limit our study to the 2D models presented in Section 2.2. The main goal is to make a connection between the two approaches used for mixing. Observe first that choosing $h(x, y) = constant$ in (2.37)-(2.39) and $L_t = L_b = 0$ in (2.40)-(2.42) leads to two strictly equivalent models. The problem discussed here is the following: given a profile $h(x, y)$, can we choose the slip lengths L_t and L_b so that the two 2D models are very close.

Recall first that

$$K_n^{2D}(x, y) = -\frac{1}{\eta}\left(\frac{h(x, y)^3}{12}\right), \qquad K_p^{2D}(x, y) = \frac{1}{\eta}\left(\frac{\overline{h}^3}{6} - \frac{\overline{h}^2}{4}(\overline{h} - 2\text{Ł})\right),$$

$$\overline{K_n^{3D}}(x, y) = -\frac{1}{\eta}\left(\frac{h(x, y)^2}{12}\right), \qquad \overline{K_p^{3D}}(x, y) = \frac{1}{\eta}\left(\frac{\overline{h}^2}{6} - \frac{\overline{h}}{4}(\overline{h} - 2\text{Ł})\right). \tag{3.55}$$

In this particular case, we supposed that the slip lengths Ł are the same at the top and bottom of the channel for K_p^{2D} and $\overline{K_p^{3D}}$. We denote by $\overline{h}$ the height of the channel in the slip pattern model. The variable length in the no slip case shall be expressed as a function of $\overline{h}$. We set $h(x, y) = \overline{h} + \tilde{h}(x, y)$. We want to find a couple of $\tilde{h}(x, y)$ and $\text{Ł}(x, y)$ that would make the results on the velocities $\overline{U_p}$ and $\overline{U_n}$ given by the two different models as close as possible.

Assuming that $h(x, y)$ is known, let us try to find $L(x, y)$ such that

$$\begin{cases} K_n^{2D}(x, y) = K_p^{2D}(x, y), \\ \overline{K_n^{3D}}(x, y) = \overline{K_p^{3D}}(x, y). \end{cases}$$

From (3.55) we have

$$\begin{cases} \dfrac{\overline{h}^3}{6} - \dfrac{\overline{h}^2}{4}(\overline{h} - 2\text{Ł}(x, y)) = -\dfrac{(\overline{h} + \tilde{h}(x, y))^3}{12}, \\ \dfrac{\overline{h}^2}{6} - \dfrac{\overline{h}}{4}(\overline{h} - 2\text{Ł}(x, y)) = -\dfrac{(\overline{h} + \tilde{h}(x, y))^2}{12}. \end{cases}$$

By multiplying the second equation by $\overline{h}$ and identifying the left hand side of each equation, we get

$$\frac{(\overline{h} + \tilde{h}(x, y))^3}{12} = \frac{\overline{h}(\overline{h} + \tilde{h}(x, y))^2}{12},$$

which implies $\tilde{h}(x, y) = 0$, which is not relevant for the application we have in mind. However, there exists a choice of parameters $\tilde{h}(x, y)$ and $\text{Ł}(x, y)$ such that, under the constraint $\tilde{h} \neq 0$, the results obtained by the two models are very close. Indeed, assuming $\tilde{h}(x, y)$ is known, let us minimize the norm of the following functional

$$F_{x,y}(L) = \begin{pmatrix} K_n^{2D}(x, y) - K_p^{2D}(x, y) \\ \overline{h}\left(\overline{K_n^{3D}}(x, y) - \overline{K_p^{3D}}(x, y)\right) \end{pmatrix}.$$

From (3.55), we have

$$F_{x,y}(\text{Ł}) = \begin{pmatrix} \dfrac{\overline{h}^3}{6} - \dfrac{\overline{h}^2}{4}(\overline{h} - 2\text{Ł}(x,y)) + \dfrac{(\overline{h} + \tilde{h}(x,y))^3}{12} \\ \dfrac{\overline{h}^3}{6} - \dfrac{\overline{h}^2}{4}(\overline{h} - 2\text{Ł}(x,y)) + \dfrac{\overline{h}(\overline{h} + \tilde{h}(x,y))^2}{12} \end{pmatrix}.$$

Denoting $c_1 = \dfrac{\overline{h}^3}{12} - \dfrac{(\overline{h} + \tilde{h}(x,y))^3}{12}$ and $c_2 = \dfrac{\overline{h}^3}{12} - \dfrac{\overline{h}(\overline{h} + \tilde{h}(x,y))^2}{12}$, $F_{x,y}(\text{Ł})$ reads

$$F_{x,y}(\text{Ł}) = \begin{pmatrix} \dfrac{\overline{h}^2}{2}\text{Ł}(x,y) - c_1 \\ \dfrac{\overline{h}^2}{2}\text{Ł}(x,y) - c_2 \end{pmatrix}.$$

In each point of the domain, let us find $\text{Ł}(x,y)$ that minimizes $||F_{x,y}(\text{Ł})||$, where $||.||$ denotes the euclidian norm. By denoting $a(s) = ||F_{x,y}(s)||$, we have

$$a(s) = \sqrt{(\dfrac{\overline{h}^2}{2}s - c_1)^2 + (\dfrac{\overline{h}^2}{2}s - c_2)^2}.$$

Since $(\dfrac{\overline{h}^2}{2}s - c_1)^2 + (\dfrac{\overline{h}^2}{2}s - c_2)^2 \neq 0$ for any acceptable s as seen above, it is possible to compute the derivative of a

$$\dfrac{\mathrm{d}a}{\mathrm{d}s}(s) = \dfrac{1}{2\sqrt{(\dfrac{\overline{h}^2}{2}s - c_1)^2 + (\dfrac{\overline{h}^2}{2}s - c_2)^2}}\left(\overline{h}^4 s - \overline{h}^2 c_1 - \overline{h}^2 c_2\right).$$

The optimum s^* satisfies

$$\dfrac{\mathrm{d}a}{\mathrm{d}s}(s^*) = 0,$$

That gives

$$\dfrac{1}{2\sqrt{(\dfrac{\overline{h}^2}{2}s^* - c_1)^2 + (\dfrac{\overline{h}^2}{2}s^* - c_2)^2}}\left(\overline{h}^4 s^* - \overline{h}^2 c_1 - \overline{h}^2 c_2\right) = 0,$$

which leads to

$$s^* = \dfrac{c_1 + c_2}{\overline{h}^2}. \tag{3.56}$$

From (3.56), the choice of Ł that minimizes the error between the coefficients of the two models in every point (x,y) of the domain is hence

$$\text{Ł}(x,y) = \dfrac{c_1 + c_2}{\overline{h}^2} = \dfrac{1}{12\overline{h}^2}(2\overline{h}^3 - (\overline{h} + \tilde{h}(x,y))^3 - \overline{h}(\overline{h} + \tilde{h}(x,y))^2),$$

that gives

$$\text{Ł}(x,y) = -\dfrac{1}{12\overline{h}^2}(\tilde{h}^3(x,y) + 4\overline{h}\tilde{h}^2(x,y) + 4\overline{h}^2\tilde{h}(x,y)). \tag{3.57}$$

It is then possible to state the following proposition.

Proposition 1. *Let $\overline{h}$ be the height of the channel. For a given function $h(x,y) = \overline{h} + \tilde{h}(x,y)$, there exists a slip length $\overline{L}(x,y)$ which minimizes the error between the*

coefficients of the two models (2.37)-(2.39) and (2.40)-(2.42). Furthermore, $\overline{L}$ is given by

$$L(x,y) = -\frac{1}{12\overline{h}^2}(\tilde{h}^3(x,y) + 4\overline{h}\tilde{h}^2(x,y) + 4\overline{h}^2\tilde{h}(x,y)).$$

Given a channel geometry $\tilde{h}(x,y)$ (see Figure 10) and the choice of $L(x,y)$ described in (3.57), we will measure the error on the results given by both models through numerical simulations.

The channels geometries are:

- For the no-slip case.
  Length $L = 1300\mu m$, width $l = 200\mu m$, maximum height $\overline{h} = 80\mu m$. We consider at the bottom of the channel a staggered herringbone geometry as described in Figure 10 with $Lc = 50\mu m$, $Lic = 100\mu m$, $\alpha = 45°$, $Gr = 50\mu m$. The height variations will vary from 0 to 50% of the total height.
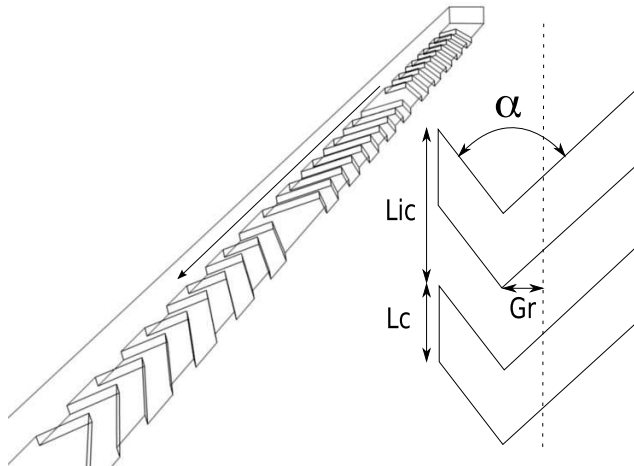
FIGURE 10. Example of a herringbone micromixer geometry

- For the patterned case.
  We use here the same geometry as described above, assuming $\overline{h}$ is constant. The slip length pattern $L(x,y)$ is calculated as described in (3.57).

As said before, we consider only one fluid in the channel. The viscosity and entry velocity are chosen such that $Re = \frac{\rho \overline{U} l}{\eta} \sim 10^{-9}$.

The discretization steps are $dx = 2.6\mu m$ and $dy = 1\mu m$ which means 20 cells per ridge in the non-planar geometry case. We ensured the discretization steps to be small enough so that the numerical error is reasonable for the comparisons we wish to do.

We define the error between the results of the two models as

$$E_r(U_p, U_n) = \frac{||U_p - U_n||_{L^2}}{||U_n||_{L^2}}.$$

Let us also introduce $\beta = \dfrac{\tilde{h}}{\bar{h}}$ the normalized height variation. As we can see in Figure 11, the results on the velocity given by the two models are fairly close for the range of β we have chosen. At most, the error is around 20% for $\beta = 0.5$. In practice we never use such height variations (1/2 of total height). In literature, most of the time $\beta \sim 0.2$ [21], which, here, generates an error lower than 10%. We can reasonably say that under the Hele-Shaw approximation, the two classical approaches for mixing enhancement studied are close.
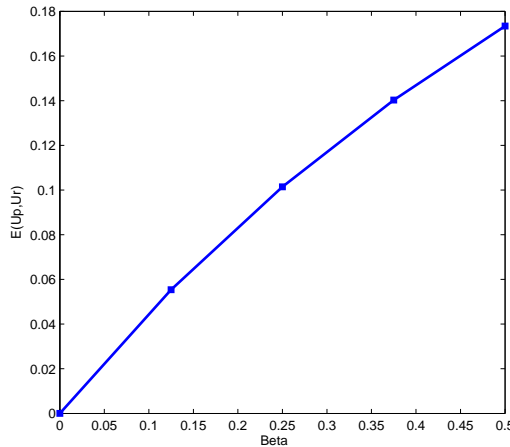
FIGURE 11. Error between the two models as a function of β

3.4.2. *Comparison between the 2.5D Reynolds model and the Stokes model for a non-flat bottom.* In order to study the validity of the 2.5D model for non planar geometry (Section 2), we compare numerical simulations performed on this model with predictions given by the Stokes model. The geometry used here is a ridge-shaped geometry, the height of the channel being given by

$$h(x, y) = h_{max} \left(1 - \frac{1 + cos(6\,\pi\,(x + 2y))}{5} \right),$$

where h_{max} is the maximum height of the channel. First, we quantify the influence of h_{max} on the error between the original Stokes model (1.1) and the 2.5D Reynolds model (2.25)-(2.27) adapted to the non-flat bottom geometry.

The error is computed on the velocities given by numerical simulations performed on both models on a $N_x \times N_y \times N_z = 400 \times 100 \times 50$ grid. The following dimensions are taken for the channel length $L = 2.5\,mm$, width $l = 500\mu m$, and h_{max} varies between $50\,\mu m$ and $200\,\mu m$.

The Figure 12 shows the expected convergence of the two models as h_{max} tends to 0. The rate of convergence shown here is 1/2.
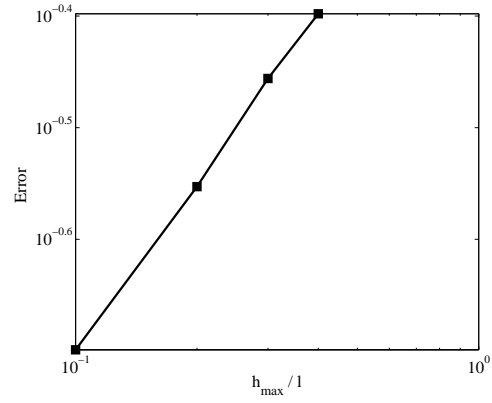
FIGURE 12. Error on the velocities given by the 2.5D Reynolds model (2.25)-(2.27) and the Stokes model (1.1), given as a function of the normalized maximum height of the channel.

The qualitative differences between the simulations performed on the two models are shown on Figure 13, by examining streamlines starting at the inlet of the channel.
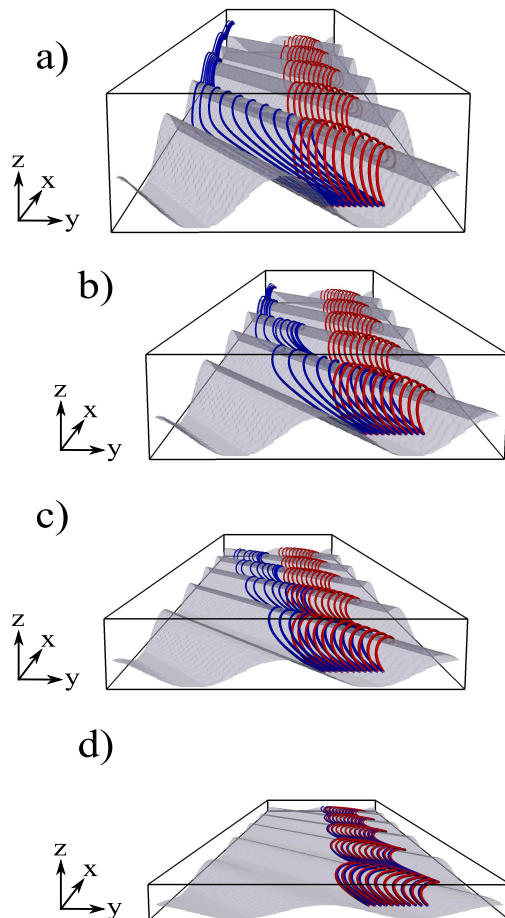
FIGURE 13. Comparison on streamlines computed from both models for various values of $h_{\max}$. a): $h_{\max} = 200\,\mu m$, b): $h_{\max} = 150\,\mu m$, c): $h_{\max} = 100\,\mu m$, d): $h_{\max} = 50\,\mu m$.

We notice that, for a sufficiently large h_{max}, the streamlines computed from the Stokes model show a deviation of the flow from the main axis of the channel to the left wall. This deviation is not seen on the Reynolds model, even though the non-flat geometry is taken into account. This deviation phenomenon is a key mechanism in fluid mixing improvement by means of microchannel geometry modification (see [17] for a complete review on micromixers). As a consequence, the Reynolds model studied in this paper is not appropriate for the study of microfluidic mixers based on this approach.

4. **Conclusion.** In this article, we have shown that the Hele-Shaw approximation (Section 2) applied to a 3D Stokes model can lead to various reduced models (Section 2.2). The main advantage of using such models is that numerical calculations are much quicker and simpler than for the full 3D Stokes model. Moreover, even though strong hypothesis are done on the microchannel geometry, these models allow us to take into account complex boundary conditions such as slip-patterned surfaces or non-planar geometries. Those kind of boundary conditions

have already been involved in various studies of enhanced fluid mixing in microchannels [21], [22] ,[13], [14]. For those reasons the reduced models developed here appear to be very interesting in general for the numerical study of flows in microchannels.

We also have shown that through this model, simulating a flow in a channel whith a complex geometry and simulating a flow in a channel patterned with hydrophilic/hydrophobic surfaces are almost equivalent (section (3.4.1)). We have seen by comparing calculations on the Hele-Shaw model with previous works [21], [22] that it doesn't describes correctly the flux deviation in the channel generated by a ridge-like shaped wall. These arguments lead us to think that chaotic mixing approaches involving a modification on the boundary conditions cannot be described using such an asymptotic reduction. A full 3D Stokes approach is needed for that.

5. **Appendix: Existence results.**

In this appendix, we consider System (2.37)-(2.39), that is we study the case of a non-flat bottom with no-slip boundary conditions in 2D. The aim is to prove the existence of weak and strong solutions to this system. The results are in the spirit of [2]. Our aim is to show how one can handle physical boundary data using maximum principle technics and extension of functions in order to prove that this kind of models gives a physically reasonable behavior of the fluid at the outlet. Our proof is not very original and the same strategy can be found in a lot of papers in the literature. The proof of existence with periodic boundary conditions or on the whole space are straightforward. The interest relies here on the boundary conditions that correspond to the physical setting: the fluids are moving because of the pressure gradient. One speaks on pressure-driven flows (see [12]).

5.1. **Existence of weak solutions.**

In this section, we deal with weak solutions. The 2D bounded rectangular domain $[0, L] \times [0, \ell]$ is denoted by Ω and its boundary is decomposed into $\Gamma = \Gamma_e \cup \Gamma_s \cup \Gamma_L$ where Γ_e is the inlet, Γ_s is the outlet and Γ_L represents the lateral walls. The outward normals of the domain are denoted by ν. We first recall the boundary conditions associated with System (2.37)-(2.39)

$$\begin{cases} \text{on } \Gamma_e, \text{ we prescribe the velocity } \overline{u} = \overline{u}_0(y) \text{ and the order parameter } \varphi = \varphi_1(y), \\ \text{on } \Gamma_s, \text{ we impose } P = 0 \text{ and } \dfrac{\partial \varphi}{\partial \nu} = 0, \\ \text{on } \Gamma_L, \text{ we assume } v = 0 \text{ and } \dfrac{\partial \varphi}{\partial \nu} = 0. \end{cases}$$

We also add the following initial condition on φ

$$\varphi(0, x, y) = \varphi_0(x, y),$$

where φ_0 is a given regular function. We also recall that, in this configuration, the coefficients K_n^{2D} and $\overline{K}_n^{3D}$ read, dropping the index n for simplicity,

$$K^{2D}(\varphi) = -\frac{h^3(x, y)}{12\eta(\varphi)}, \quad \overline{K}^{3D}(\varphi) = -\frac{h^2(x, y)}{12\eta(\varphi)},$$

where $\eta(s) = \eta_1 s + \eta_2(1 - s)$ for all $s \in [0, 1]$. As a consequence, there exists two positive constants K_1 and K_2 such that

$$\forall s \in [0, 1], \ K_1 \le \left|K^{2D}(s)\right| \le K_2, \ \ K_1 \le \left|\overline{K}^{3D}(s)\right| \le K_2, \ \ K_1 \le \left|K^{'2D}(s)\right| \le K_2, \ K_1 \le \left|K^{'3D}(s)\right| \le K_2,$$
$$(5.58)$$

where $K^{'2D}$ and $K^{'3D}$ denote the derivative of K^{2D} and K^{3D}. We now can state the following theorem.

Theorem 5.1. *Assume that $D(\varphi)$ is constant, $\varphi_1(y) \in H^2(0, \ell)$, $\frac{\partial \varphi_1}{\partial \nu} = 0$ on Γ_L, $\overline{u}_0(y) \in L^2(0, \ell)$, $\overline{u}_0 \geq 0$ and $\varphi_0 \in L^2(\Omega)$ such that $0 \leq \varphi_0 \leq 1$. Then there exists a global weak solution $(P, \overline{u}, \overline{v}, \varphi)$ to System (2.37)-(2.39) such that $\varphi(0, x, y) = \varphi_0(x, y)$ and*

$$P \in L^2_{loc}\Big(\mathbb{R}_+; H^1(\Omega)\Big),$$

$$(\overline{u}, \overline{v}) \in \Big[L^2_{loc}\Big(\mathbb{R}_+; H^1(\Omega)\Big)\Big]^2,$$

$$\varphi \in L^\infty_{loc}\Big(\mathbb{R}_+; L^2(\Omega)\Big) \cap L^2_{loc}\Big(\mathbb{R}_+; H^1(\Omega)\Big),$$

Proof. The proof is based on a Galerkin method. To this end, we first get rid of the inhomogeneous Dirichlet boundary condition φ_1 at the inlet by introducing the following change of unknow $\phi = \varphi - \varphi_1$. Since coefficient D is constant, System (2.37)-(2.39) is transformed into

$$
\begin{cases}
\nabla_{xy} \cdot \Big(K^{2D}(\varphi_1 + \phi)\nabla_{x,y}P(x,y)\Big) = 0, & (5.59) \\[2mm]
\begin{pmatrix} \overline{u} \\ \overline{v} \end{pmatrix} = \overline{K}^{3D}(\varphi_1 + \phi)\nabla_{xy}P, & (5.60) \\[2mm]
\partial_t \phi + \begin{pmatrix} \overline{u} \\ \overline{v} \end{pmatrix} \cdot \nabla\phi - D\Delta_{x,y}\phi = -\overline{v}\partial_y\varphi_1 + D\partial_y^2\varphi_1. & (5.61)
\end{cases}
$$

Note that ϕ satisfies the homogeneous Neumann boundary condition

$$\frac{\partial \phi}{\partial \nu} = 0$$

at the outlet and on the lateral walls provided that the compatibility condition

$$\frac{\partial \varphi_1}{\partial \nu} = 0$$

holds on lateral walls. The boundary conditions for $(P, \overline{u}, \overline{v}, \phi)$ then read

$$
\begin{cases}
\text{on } \Gamma_e, \ \overline{u} = \overline{u}_0(y), \ \phi = 0, \\[2mm]
\text{on } \Gamma_s, \ P = 0 \text{ and } \frac{\partial \phi}{\partial \nu} = 0, \\[2mm]
\text{on } \Gamma_L, \ \overline{v} = 0 \text{ and } \frac{\partial \phi}{\partial \nu} = 0.
\end{cases}
\qquad (5.62)
$$

We now introduce the Galerkin basis associated with the eigenfunctions of the Laplacian operator on Ω with the boundary conditions satisfied by ϕ, namely

$$\forall (i,j) \in \mathbb{N}^2, \ e_{ij}(x,y) = \sin\Big((i + \frac{1}{2})\frac{\pi x}{L}\Big)\cos\Big(j\frac{\pi y}{l}\Big).$$

We first reorganized the sequence $\Big(e_{ij}\Big)_{i,j\in\mathbb{N}^2}$ to obtain $\Big(e_n\Big)_{N\in\mathbb{N}}$ and introduce the finite dimensional space V_n spanned by $\Big(e_k\Big)_{0\leq k\leq n}$. The approximate solution

$\left(P_n, \overline{u}_n, \overline{v}_n, \phi_n\right)$ is given by $\phi_n \in V_n$ and

$$\begin{cases} \nabla_{xy} \cdot \left(K^{2D}(\varphi_1 + \phi_n)\nabla_{x,y}P_n(x,y)\right) = 0, & (5.63) \\[2mm] \begin{pmatrix} \overline{u}_n \\ \overline{v}_n \end{pmatrix} = \overline{K}^{3D}(\varphi_1 + \phi_n)\nabla_{xy}P_n, & (5.64) \\[2mm] \forall 0 \le k \le n, \ \int_\Omega \partial_t \phi_n e_k + \int_\Omega \begin{pmatrix} \overline{u}_n \\ \overline{v}_n \end{pmatrix} \cdot \nabla \phi_n e_k - D\int_\Omega \Delta_{x,y}\phi_n e_k = \int_\Omega \left(-\overline{v}_n \partial_y \varphi_1 + D\partial_y^2 \varphi_1\right)e_k & (5.65) \end{cases}$$

It is clear that System of ODE's (5.63)-(5.65) admits a unique solution $\left(P_n, \overline{u}_n, \overline{v}_n, \phi_n\right)$ on a time intervall $[0, T_n[$, with $T_n > 0$. To conclude the proof of Theorem 5.1, it remains to show that $T_n = +\infty$ and to perform the limit $n \to +\infty$ into (5.63)-(5.64). To this end, we need a priori estimates on $\left(P_n, \overline{u}_n, \overline{v}_n, \phi_n\right)$. Let us write

$$\forall t \in [0, T_n[, \ \phi_n(t) = \sum_{k=0}^{n} \alpha_k(t)e_k,$$

and multiply Equation (5.65) by α_k to obtain , after summation,

$$\int_\Omega \partial_t \phi_n \phi_n + \int_\Omega \begin{pmatrix} \overline{u}_n \\ \overline{v}_n \end{pmatrix} \cdot \nabla \phi_n \phi_n - D\int_\Omega \Delta_{x,y}\phi_n \phi_n = \int_\Omega \left(-\overline{v}_n \partial_y \varphi_1 + D\partial_y^2 \varphi_1\right)\phi_n$$

$$(5.66)$$

An integration by parts gives, recalling that

$$\nabla \cdot \begin{pmatrix} \overline{u}_n \\ \overline{v}_n \end{pmatrix} = 0, \tag{5.67}$$

$$\frac{1}{2}\partial_t \int_\Omega \phi_n^2 + \frac{1}{2}\int_\Gamma \begin{pmatrix} \overline{u}_n \\ \overline{v}_n \end{pmatrix} \cdot \vec{\nu} \, \phi_n^2 + D\int_\omega |\nabla \phi_n|^2 - \int_\Gamma \nabla \phi_n \cdot \vec{\nu} \, \phi_n = \int_\Omega \left(-\overline{v}_n \partial_y \varphi_1 + D\partial_y^2 \varphi_1\right)\phi_n.$$

$$(5.68)$$

Using (5.62), we have

$$\int_\Gamma \nabla \phi_n \cdot \vec{\nu} \, \phi_n = 0,$$
$$\int_\Gamma \begin{pmatrix} \overline{u}_n \\ \overline{v}_n \end{pmatrix} \cdot \vec{\nu} \, \phi_n^2 = \int_{\Gamma_s} \overline{u}_n(L) \, \phi_n^2. \tag{5.69}$$

We then need the following lemma.

Lemma 5.2. *The solution $\overline{u}_n$ to Equation (5.64) satisfies $\overline{u}_n(t, L, y) \ge 0$, for all $t \in [0, T_n[$ and $y \in [0, \ell]$.*

Proof. We begin with the positivity of P_n in the domain Ω. We decompose P_n in the following way $P_n = P_n^+ + P_n^-$ where P_n^+ (resp. P_n^-) denotes the positive part (resp. the negative part) of P_n. Multiply Equation (5.63) by P_n^-, we obtain

$$-\int_\Omega K^{2D}(\varphi_1 + \phi_n)|\nabla P_n^-|^2 + \int_\Gamma K^{2D}(\varphi_1 + \phi_n)\frac{\partial P_n}{\partial \nu}P_n^- = 0.$$

Using (5.62) and Equation (5.64), we then derive

$$-\int_\Omega K^{2D}(\varphi_1 + \phi_n)|\nabla P_n^-|^2 - \int_{\Gamma_e} K^{2D}(\varphi_1)\frac{\overline{u}_0(y)}{\overline{K}^{3D}(\varphi_1(y))}P_n^- = 0.$$

Since $\overline{K}^{2D}(\varphi_1(y)) \leq 0$, $\overline{K}^{3D}(\varphi_1(y)) \leq 0$, and $\overline{u}_0(y) \geq 0$, one can see that

$$\int_{\Gamma_e} K^{2D}(\varphi_1) \frac{\overline{u}_0(y)}{\overline{K}^{3D}(\varphi_1(y))} P_n^- \leq 0,$$

which implies that

$$\int_\Omega K^{2D}(\varphi_1 + \phi_n)|\nabla P_n^-|^2 = 0.$$

It follows that $|\nabla P_n^-| = 0$ and then $P_n^- = 0$. As a consequence, $P_n \geq 0$ in the domain Ω. Furthermore, since on Γ_s, one has $P_n = 0$, one deduces that on Γ_s

$$\frac{\partial P_n}{\partial x} \leq 0.$$

Recalling that, according to equation (5.64), on Γ_s, one has

$$\overline{u}_n(L, y) = \overline{K}^{3D}(\varphi_1 + \phi_n)\frac{\partial P_n}{\partial x},$$

the result follows from the fact that $\overline{K}^{3D}(\varphi_1 + \phi_n) \leq 0$. $\qquad\square$

Remark 2. *Lemma 5.2 states that for any smooth solution to (5.59)-(5.61), the velocity is directed toward the exterior of the channel at the outlet.*

Equipped with Lemma 5.2, we are also able to derive the following maximum principle for ϕ_n.

Lemma 5.3. *Let ϕ_n be the solution to Equation (5.66). Then ϕ_n satisfies $0 \leq \phi_n \leq 1$ on Ω.*

Proof. We use the notation of Lemma 5.2 and decompose $\phi_n = \phi_n^+ + \phi_n^-$. We multiply Equation (5.66) by ϕ_n^- and we integrate over Ω. A straightforward integration by parts gives

$$\frac{1}{2}\partial_t \int_\Omega \left(\phi_n^-\right)^2 + \frac{1}{2}\int_\Gamma \left(\frac{\overline{u}_n}{\overline{v}_n}\right) \cdot \vec{\nu} \left(\phi_n^-\right)^2 + D\int_\Omega |\nabla \phi_n^-|^2 - D\int_\Gamma \nabla \phi_n^- \cdot \vec{\nu}\, \phi_n^- = 0. \tag{5.70}$$

Using the boundary conditions (5.62) on ϕ and Lemma 5.2, we derive

$$\int_\Gamma \nabla \phi_n^- \cdot \vec{\nu}\, \phi_n^- = 0, \quad \int_\Gamma \left(\frac{\overline{u}_n}{\overline{v}_n}\right) \cdot \vec{\nu} \left(\phi_n^-\right)^2 = \int_{\Gamma_e} \overline{u}_n(L)\left(\phi_n^-\right)^2 \geq 0.$$

Then (5.70) provides

$$\partial_t \int_\Omega \left(\phi_n^-\right)^2 \leq 0.$$

We thus obtain $\phi_n^- = 0$ since at $t = 0$, $\phi_n \geq 0$, which implies that $\phi_n \geq 0$ on Ω. In order to conclude the proof of Lemma 5.3, it remains to prove that $\phi \leq 1$ on Ω which is done by performing the same computation with $\tilde{\phi} = 1 - \phi$. $\qquad\square$

We are now able to end the proof of Theorem 5.1. From (5.68), we derive, using Lemma 5.2, (5.69) and Cauchy-Schwarz inequality

$$\frac{1}{2}\partial_t \int_\Omega \phi_n^2 + D\int_\omega |\nabla \phi_n|^2 \leq C_1\left(||\overline{v}_n||_2 + 1\right)||\phi_n||_2, \tag{5.71}$$

where the constant C_1 depends on $||\varphi_1||_{H^2(0,D)}$. Using (5.58), a priori estimates on Equations (5.63) and (5.64) are straightforward and leads to the existence of a constant C_2 such that

$$||P_n(t)||_{L^2(0,T_n;H^1(\Omega))} + ||(\overline{u},\overline{v})||_{L^2(0,T_n;L^2(\Omega))} \leq C_2. \qquad (5.72)$$

Then by Gronwall Lemma's, we deduce from (5.71) that ϕ_n is bounded in $L^\infty_{\text{loc}}\left(\mathbb{R}_+; L^2(\Omega)\right) \cap L^2_{\text{loc}}\left(\mathbb{R}_+; H^1(\Omega)\right)$ and that $T_n = +\infty$. It remains to perform the limit $n \to +\infty$ in the weak formulation (5.63)-(5.65) which is done by using

$$\nabla \cdot \begin{pmatrix} \overline{u}_n \\ \overline{v}_n \end{pmatrix} = 0,$$

and the Aubin-Simon compactness lemma (see [20]) which provides a strong convergence of $\left(\phi_n\right)_{n\in\mathbb{N}}$ in $L^\infty\left(0,T; L^2(\Omega)\right)$ for all $T > 0$. $\qquad \square$

5.2. **Existence of strong solutions.** In this section, we prove the existence of strong solutions to System (2.37)-(2.39). The main result presented here reads

Theorem 5.4. *Assume that $D(\phi)$ is constant, $\varphi_1(y) \in H^3(0,\ell)$, $\frac{\partial\varphi_1}{\partial\nu} = 0$ on Γ, $\overline{u}_0(y) \in H^1(0,\ell)$, $\overline{u}_0 \geq 0$, $\partial_y\overline{u}_0 = 0$ on lateral walls and $\varphi_0 \in H^1(\Omega)$ such that $\varphi_0 = \varphi_1$ on Γ_e and $0 \leq \varphi_0 \leq 1$. Then there exists a time $T > 0$ and a unique solution $(P, \overline{u}, \overline{v}, \varphi)$ to System (2.24)-(2.27) such that $\varphi(0) = \varphi_0$ and*

$$P \in L^\infty\left(0,T; H^2(\Omega)\right), \quad (\overline{u},\overline{v}) \in \left(L^\infty\left(0,T; H^1(\Omega)\right)\right)^2$$
$$\varphi \in L^\infty\left(0,T; H^1(\Omega)\right) \cap L^2\left(0,T; H^2(\Omega)\right).$$

Proof. As in the proof of Theorem 5.1, we first perform the change of unknown $\varphi = \varphi_1 + \phi$ to obtain System (5.59)-(5.61) with boundary conditions (5.62). The proof is based on the Galerkin method used in Section 5.1. For that reason, we give here a sketch of the proof by performing only the a priori estimates on ϕ (see Section 5.1 for more details). From now on, for simplicity, we drop the index n in the different unknowns. We first recall the following inequality stated when the space dimension is equal to 2

$$\exists\, C > 0, \; \forall \psi \in H^1(\Omega), ||\psi||_4 \leq C||\psi||_2^{\frac{1}{2}}||\psi||_{H^1}^{\frac{1}{2}}. \qquad (5.73)$$

Repeating the computation of Section 5.1, we first obtain a bound for ϕ in $L^\infty\left(0,T; L^2(\Omega)\right) \cap L^2\left(0,T; H^1(\Omega)\right)$, for P in $L^\infty\left(0,T; H^1(\Omega)\right)$ and $(\overline{u},\overline{v})$ in $L^2\left(0,T; L^2(\Omega)\right)$. In order to estimate $\nabla\phi$, we introduce the equations satisfied by $\partial_x\phi$ and $\partial_y\phi$

$$\partial_t\left(\partial_x\phi\right) + \begin{pmatrix} \overline{u} \\ \overline{v} \end{pmatrix} \cdot \nabla\left(\partial_x\phi\right) - D\Delta\left(\partial_x\phi\right) + \partial_x\begin{pmatrix} \overline{u} \\ \overline{v} \end{pmatrix} \cdot \nabla\phi = -\partial_x\overline{v}\partial_y\varphi_1, \qquad (5.74)$$

$$\partial_t\left(\partial_y\phi\right) + \begin{pmatrix} \overline{u} \\ \overline{v} \end{pmatrix} \cdot \nabla\left(\partial_y\phi\right) - D\Delta\left(\partial_y\phi\right) + \partial_y\begin{pmatrix} \overline{u} \\ \overline{v} \end{pmatrix} \cdot \nabla\phi = -\partial_y\overline{v}\partial_y\varphi_1 - \overline{v}\partial_y^2\varphi_1 + D\partial_y^3\varphi_1.$$
$$(5.75)$$

We multiply Equations (5.74) and (5.75) by respectively $\partial_x \phi$ and $\partial_y \phi$ and integrate over Ω the resulting equations to get

$$\frac{1}{2}\partial_t \int_\Omega |\partial_x \phi|^2 + \frac{1}{2}\int_\Gamma |\partial_x \phi|^2 \left(\frac{\overline{u}}{\overline{v}}\right) \cdot \nu + D\int_\Omega |\nabla \partial_x \phi|^2 - D\int_\Gamma \partial_\nu(\partial_x \phi)\,\partial_x \phi + \int_\Omega \partial_x \left(\frac{\overline{u}}{\overline{v}}\right) \cdot \nabla \phi\, \partial_x \phi = -\int_\Omega \partial_x \overline{v}\partial_y \varphi_1 \partial$$
$$(5.76)$$

$$\frac{1}{2}\partial_t \int_\Omega |\partial_y \phi|^2 + \frac{1}{2}\int_\Gamma |\partial_y \phi|^2 \left(\frac{\overline{u}}{\overline{v}}\right) \cdot \nu + D\int_\Omega |\nabla \partial_y \phi|^2 - D\int_\Gamma \partial_\nu(\partial_y \phi)\partial_y \phi + \int_\Omega \partial_y \left(\frac{\overline{u}}{\overline{v}}\right) \cdot \nabla \phi\, \partial_y \phi$$
$$= -\int_\Omega \partial_y \overline{v}\partial_y \varphi_1 \partial_y \phi. + \int_\Omega \left(-\overline{v}\partial_y^2 \varphi_1 + D\partial_y^3 \varphi_1\right)\partial_y \phi, \qquad (5.77)$$

Using (5.62) and the fact that since $\phi \in V_n$, one has $\partial_x^2 \phi = 0$ on Γ_e, we have

$$\int_\Gamma \partial_\nu(\partial_x \phi)\,\partial_x \phi = 0, \qquad (5.78)$$

and

$$\int_\Gamma |\partial_x \phi|^2 \left(\frac{\overline{u}}{\overline{v}}\right) \cdot \nu = -\int_{\Gamma_e} |\partial_x \phi|^2 \overline{u}_0(y). \qquad (5.79)$$

Plugging (5.78) and (5.79) into (5.76), we get

$$\frac{1}{2}\partial_t \int_\Omega |\partial_x \phi|^2 + D\int_\Omega |\nabla \partial_x \phi|^2 \leq ||\partial_x(\overline{u},\overline{v})||_2||\nabla \phi||_4||\partial_x \phi||_4 + C||\partial_x \overline{v}||_2||\partial_x \phi||_2 + C||\partial_x \phi||_2||\nabla \partial_x \phi||_2,$$
$$(5.80)$$

where the constant C depends only on φ_1 and u_0. Again, dealing with (5.77), the boundary conditions (5.62) provides

$$\int_\Gamma \partial_\nu(\partial_y \phi)\,\partial_y \phi = 0,$$

$$\int_\Gamma |\partial_y \phi|^2 \left(\frac{\overline{u}}{\overline{v}}\right) \cdot \nu = \int_{\Gamma_s} |\partial_y \phi|^2 \overline{u}_0(L),$$

which leads to

$$\frac{1}{2}\partial_t \int_\Omega |\partial_y \phi|^2 + \frac{1}{2}\int_{\Gamma_s} |\partial_y \phi|^2 \overline{u}(L) + D\int_\Omega |\nabla \partial_y \phi|^2$$

$$\leq ||\partial_y(\overline{u},\overline{v})||_2||\nabla \phi||_4||\partial_y \phi||_4 + C||\partial_y \overline{v}||_2||\partial_y \phi||_2 + C\left(||\overline{v}||_2 + 1\right)||\partial_y \phi||_2, \quad (5.81)$$

where the constant C depends only on φ_1. By Lemma 5.2, one has $\overline{u}(L) \geq 0$ on Γ_s, then summing Inequalities (5.80) and (5.81) leads to

$$\frac{1}{2}\partial_t \int_\Omega |\nabla \phi|^2 + D\int_\Omega \left(|\nabla \partial_x \phi|^2 + |\nabla \partial_y \phi|^2\right)$$

$$\leq 2||\nabla(\overline{u},\overline{v})||_2||\nabla \phi||_4^2 + C\left(1 + ||\overline{v}||_2 + ||\nabla \overline{v}||_2\right)||\nabla \phi||_2 + C||\nabla \phi||_2||\nabla \partial_x \phi||_2.$$
$$(5.82)$$

Using (5.73), we then obtain

$$\frac{1}{2}\partial_t \int_\Omega |\nabla \phi|^2 + D\int_\Omega \left(|\nabla \partial_x \phi|^2 + |\nabla \partial_y \phi|^2\right)$$

$$\leq C||\nabla(\overline{u},\overline{v})||_2||\nabla \phi||_2||\phi||_{H^2} + C\left(1 + ||\overline{v}||_{H^1}\right)||\nabla \phi||_2 + C||\phi||_{H^1}||\phi||_{H^2}, \quad (5.83)$$

where the constant C depends only on $\overline{u}_0$ and φ_1. It remains to control $\nabla\overline{u}$ and $\nabla\overline{v}$ in $L^2(\Omega)$ and this is done in the following lemma.

Lemma 5.5. *There exists a constant C depending only on φ_1, $\overline{u}_0$ such that*

$$||\overline{u}||_{H^1} + ||\overline{v}||_{H^1} \leq C\big(1 + (1 + ||\phi||_{H^1})||\phi||_{H^2}\big).$$

Proof. We proceed in two steps.

• **Step 1:** Estimates on P. We first recall that multiplying Equation (5.59) by P, integrating by parts and using (5.58) and (5.62), we obtain an H^1-bound on P which reads as follows

$$\forall t \in [0, T], \ ||P(t)||_{H^1} \leq C, \tag{5.84}$$

where the constant C depends only on $\overline{u}_0$. We apply ∂_y on Equation (5.59) to get

$$\nabla \cdot \left(K^{'2D}(\varphi_1 + \phi)\partial_y(\varphi_1 + \varphi)\nabla P \right) + \nabla \cdot \left(K^{2D}(\varphi_1 + \phi)\nabla\partial_y P \right) = 0. \tag{5.85}$$

Multiplying Equation (5.85) by $\partial_y P$ leads to, after integration over Ω:

$$\int_\Omega K^{'2D}(\varphi_1 + \phi)\partial_y(\varphi_1 + \varphi)\nabla P \cdot \nabla\big(\partial_y P\big) - \int_\Gamma K^{'2D}(\varphi_1 + \phi)\partial_y(\varphi_1 + \varphi)\nabla P \cdot \nu \, \partial_y P$$

$$+ \int_\Omega K^{2D}(\varphi_1 + \phi)|\nabla\partial_y P|^2 - \int_\Gamma K^{2D}(\varphi_1 + \phi)\nabla\big(\partial_y P\big) \cdot \nu \, \partial_y P = 0. \tag{5.86}$$

Using (5.62) and Equation (5.59), recalling in particular that $\phi = 0$ on Γ_e, one can write

$$\int_\Gamma K^{'2D}(\varphi_1 + \phi)\partial_y(\varphi_1 + \varphi)\nabla P \cdot \nu \, \partial_y P = -\int_{\Gamma_e} K^{'2D}(\varphi_1)\partial_y\varphi_1\frac{\overline{u}_0(y)}{\overline{K}^{3D}(\varphi_1)}\partial_y P \tag{5.87}$$

$$\int_\Gamma K^{2D}(\varphi_1 + \phi)\nabla\big(\partial_y P\big) \cdot \nu \, \partial_y P = -\int_{\Gamma_e} K^{2D}(\varphi_1)\partial_y\left(\frac{\overline{u}_0(y)}{\overline{K}^{3D}(\varphi_1)}\right)\partial_y P. \tag{5.88}$$

Using (5.87), (5.88) and Cauchy-Schwarz inequality, we then obtain from (5.86)

$$\int_\Omega K^{2D}(\varphi_1 + \phi)|\nabla\partial_y P|^2 \leq C\left(||\partial_y\phi||_4 + 1\right)||\nabla P||_4||\nabla\partial_y P||_2 + \int_{\Gamma_e}\left|K^{'2D}(\varphi_1)\,\partial_y\varphi_1\frac{\overline{u}_0(y)}{\overline{K}^{3D}(\varphi_1)}\partial_y P\right|$$

$$+ \int_{\Gamma_e}\left|K^{2D}(\varphi_1)\partial_y\left(\frac{\overline{u}_0(y)}{\overline{K}^{3D}(\varphi_1)}\right)\partial_y P\right|, \tag{5.89}$$

where C depends only on φ_1. Using (5.58), (5.73) in (5.89), the trace Theorem and the H^1-bound (5.84) on P, we get

$$\int_\Omega |\nabla\partial_y P|^2 \leq C||\phi||_{H^1}^{\frac{1}{2}}||\phi||_{H^2}^{\frac{1}{2}}||P||_{H^1}^{\frac{1}{2}}||P||_{H^2}^{\frac{3}{2}} + C||P||_{H^1}^{\frac{1}{2}}||P||_{H^2}^{\frac{3}{2}}, +C||P||_{H^1}^{\frac{1}{2}}||P||_{H^2}^{\frac{1}{2}}$$

$$\leq C||\phi||_{H^1}^{\frac{1}{2}}||\phi||_{H^2}^{\frac{1}{2}}||P||_{H^2}^{\frac{3}{2}} + C\big(||P||_{H^2}^{\frac{3}{2}} + ||P||_{H^2}^{\frac{1}{2}}\big), \tag{5.90}$$

where the constant C depends only on $\overline{u}_0$ and φ_1.

Applying ∂_x on Equation (5.59), we derive, recalling that φ_1 does not depend on x

$$\nabla \cdot \left(K^{2D}(\varphi_1 + \phi)\nabla\partial_x P \right) + \nabla \cdot \left(K^{'2D}(\varphi_1 + \phi)\partial_x\phi\nabla P \right) = 0. \tag{5.91}$$

Note that at the inlet, we don't have any information on $\partial_x \phi$. To overcome this difficulty, we introduce an extension of P in the following sense. Denote

$$Q = P - \frac{1}{\overline{K}^{3D}(\varphi_1 + \phi)}\overline{u}_0 f(x), \tag{5.92}$$

where f is a smooth function satisfying $f(0) = f(L) = f'(L) = f''(L) = 0$ and $f'(0) = 1$. Then, there exists a constant $C > 0$ depending on φ_1, $\overline{u}_0$ and f such that

$$||P||_{H^2} \leq C||\phi||_{H^2} + ||Q||_{H^2}, \quad ||Q||_{H^2} \leq C||\phi||_{H^2} + ||P||_{H^2}. \tag{5.93}$$

The equation for Q is

$$\nabla \cdot \left(K^{2D}(\varphi_1 + \phi)\nabla\partial_x Q\right) + \nabla \cdot \left(K^{2D}(\varphi_1 + \phi)\nabla\partial_x(\frac{1}{\overline{K}^{3D}(\varphi_1 + \phi)}\overline{u}_0 f(x))\right)$$

$$+\nabla \cdot \left(K'^{2D}(\varphi_1 + \phi)\partial_x\phi\nabla P\right) = 0. \tag{5.94}$$

The energy estimate on Equation (5.94) reads

$$-\int_\Omega K^{2D}(\varphi_1 + \phi)|\nabla\partial_x Q|^2 - \int_\Omega K^{2D}(\varphi_1 + \phi)\left(\nabla\partial_x(\frac{1}{\overline{K}^{3D}(\varphi_1 + \phi)}\overline{u}_0 f(x))\right) \cdot \nabla\partial_x Q$$

$$-\int_\Omega K'^{2D}(\varphi_1 + \phi)\partial_x\phi\nabla P \cdot \nabla\partial_x Q + \int_\Gamma K^{2D}(\varphi_1 + \phi)(\nabla\partial_x Q) \cdot \vec{\nu}\,\partial_x Q$$

$$+\int_\Gamma K^{2D}(\varphi_1 + \phi)\left(\nabla\partial_x(\frac{1}{\overline{K}^{3D}(\varphi_1 + \phi)}\overline{u}_0 f(x))\right) \cdot \vec{\nu}\,\partial_x Q + \int_\Gamma K'^{2D}(\varphi_1 + \phi)\partial_x\phi\nabla P \cdot \vec{\nu}\,\partial_x Q = 0. \tag{5.95}$$

Here, the boundary terms have to be computed seperately and carefully. The boundary conditions on Q are the following ones. On the lateral walls, we have $\partial_y P = 0$. This implies $\partial_x\partial_y P = 0$ since ∂_x is a tangential derivative on Γ_L. We then need the compatibility condition

$$\partial_y\left(\frac{1}{\overline{K}^{3D}(\varphi_1 + \phi)}\overline{u}_0 f(x)\right) = 0, \tag{5.96}$$

at the boundary, which is satisfied since on lateral walls $\partial_y\phi = 0$, $\partial_y\varphi_1 = 0$ and $\partial_y\overline{u}_0 = 0$ by hypothesis (see Theorem 5.4). This yields, on Γ_L,

$$\partial_y Q = 0, \ \partial_x\partial_y Q = 0.$$

At the inlet Γ_e, one can write using Equation (5.60) and (5.62),

$$\partial_x P = \frac{1}{\overline{K}^{3D}(\varphi_1)}\overline{u}_0,$$

which provides

$$\partial_x Q = \frac{1}{\overline{K}^{3D}(\varphi_1)}\overline{u}_0(y) - \frac{1}{\overline{K}^{3D}(\varphi_1)}\overline{u}_0(y)f'(0) - \partial_x\left(\frac{1}{\overline{K}^{3D}(\varphi_1)}\right)\overline{u}_0(y)f(x) = 0,$$

since $f(0) = 0$ and $f'(0) = 1$. At the outlet, $P = 0$ implies that $\partial_y P = \partial_y^2 P = 0$. By Equation (5.59), we deduce

$$K^{2D}(\varphi_1 + \phi)\Delta P + K'^{2D}(\varphi_1 + \phi)\nabla(\varphi_1 + \phi) \cdot \nabla P = 0.$$

Since, on Γ_s, $\partial_x(\varphi_1 + \phi) = 0$ and $K^{2D}(\varphi_1 + \phi) \neq 0$, we have

$$\partial_x^2 P = -\partial_y^2 P = 0.$$

Then

$$\partial_x^2 Q = -\partial_x^2 \Big(\frac{1}{\overline{K}^{3D}(\varphi_1 + \phi)} \overline{u}_0(y) f(x) \Big),$$

$$= -\partial_x^2 \Big(\frac{1}{\overline{K}^{3D}(\varphi_1 + \phi)} \Big) \overline{u}_0(y) f(x) - 2\partial_x \Big(\frac{1}{\overline{K}^{3D}(\varphi_1 + \phi)} \Big) \overline{u}_0(y) f'(x) - \frac{1}{\overline{K}^{3D}(\varphi_1 + \phi)} \overline{u}_0(y) f''(x).$$

Taking $x = L$ in the last equality and since $f(L) = f'(L) = f''(L) = 0$, one concludes that $\partial_x^2 Q = 0$ on Γ_s. As a consequence, we deduce, using also (5.62), that

$$\int_\Gamma K^{2D}(\varphi_1 + \phi)(\nabla \partial_x Q) \cdot \vec{\nu} \, \partial_x Q = 0, \qquad (5.97)$$

$$\int_\Gamma K^{2D}(\varphi_1 + \phi) \Big(\nabla \partial_x \Big(\frac{1}{\overline{K}^{3D}(\varphi_1 + \phi)} \overline{u}_0 f(x) \Big) \Big) \cdot \vec{\nu} \, \partial_x Q = 0, \qquad (5.98)$$

$$\int_\Gamma K'^{2D}(\varphi_1 + \phi) \partial_x \phi \nabla P \cdot \vec{\nu} \, \partial_x Q = 0. \qquad (5.99)$$

Collecting (5.97), (5.98) and (5.99), we obtain from (5.95)

$$-\int_\Omega K^{2D}(\varphi_1 + \phi)|\nabla \partial_x Q|^2 - \int_\Omega K^{2D}(\varphi_1 + \phi) \Big(\nabla \partial_x \Big(\frac{1}{\overline{K}^{3D}(\varphi_1 + \phi)} \overline{u}_0 f(x) \Big) \Big) \cdot \nabla \partial_x Q$$

$$-\int_\Omega K'^{2D}(\varphi_1 + \phi) \partial_x \phi \nabla P \cdot \nabla \partial_x Q = 0, \qquad (5.100)$$

which leads, by Cauchy-Schwarz inequality and using (5.58), to

$$\int_\Omega |\nabla \partial_x Q|^2 \le C||\phi||_{H^2}||\nabla \partial_x Q||_2 + C||\partial_x \phi||_4||\nabla P||_4||\nabla \partial_x Q||_2 \qquad (5.101)$$

$$\le C||\phi||_{H^2}||Q||_{H^2} + C||\phi||_{H^1}^{\frac{1}{2}}||\phi||_{H^2}^{\frac{1}{2}}||P||_{H^1}^{\frac{1}{2}}||P||_{H^2}^{\frac{1}{2}}||Q||_{H^2}, \qquad (5.102)$$

thanks to Inequality (5.73). Then, by (5.84) and (5.93), there exists a constant C depending only on φ_1, $\overline{u}_0$ and f and a small constant α such that

$$\int_\Omega |\nabla \partial_x P|^2 \le \alpha||P||_{H^2}^2 + C\Big(1 + \big(1 + ||\phi||_{H^1}^2 \big)||\phi||_{H^2}^2 \Big). \qquad (5.103)$$

Collecting (5.90) and (5.103), we conclude by Hölder inequality that

$$||P||_{H^2}^2 \le C\Big(1 + \big(1 + ||\phi||_{H^1}^2 \big)||\phi||_{H^2}^2 \Big). \qquad (5.104)$$

• **Step 2:** Conclusion. Back to Equation (5.60), we prove directly using (5.58) that there exists a constant $C = C(\varphi_1, \overline{u}_0, f)$ such that

$$||\overline{u}||_{H^1} + ||\overline{v}||_{H^1} \le C\Big(1 + (1 + ||\phi||_{H^1})||\phi||_{H^2} \Big). \qquad (5.105)$$

□

From estimate (5.83), we obtain using Lemma 5.5 and recalling that ϕ is bounded in $L^\infty \Big(0, T; L^2(\Omega) \Big) \cap L^2 \Big(0, T; H^1(\Omega) \Big)$

$$\frac{1}{2}\partial_t \int_\Omega |\nabla \phi|^2 + D \int_\Omega \Big(|\nabla \partial_x \phi|^2 + |\nabla \partial_y \phi|^2 \Big) \le C\Big(1 + ||\phi||_{H^2} + ||\phi||_{H^2}^2 \Big). \qquad (5.106)$$

We conclude by Gronwall's lemma that ϕ is bounded in $L^\infty\Big(0,T;H^1(\Omega)\Big)\cap L^2\Big(0,T;H^2(\Omega)\Big)$, which concludes the proof of Theorem 5.4. $\square$

REFERENCES

[1] G. Bayada and M. Chambat, *New models in the theory of the hydrodynamic bifurcation of rough surfaces*, J. Tribol., **110**, (1988), 402-407.

[2] F. Boyer, *Mathematical study of multiphase flow under shear trhough order parameter formulation*, Asymptotic Analysis, **20(2)**, (1999), 175-212.

[3] F. Boyer and P. Fabrie, *Eléments d'analyse pour l'étude de quelques modèles d'écoulements de fluides visqueux incompressibles*, Spinger, (2006).

[4] D. Bresch, C. Choquet, L. Chupin, T. Colin, M. Gisclon, *Roughness-induced effect at main order on the Reynolds approximation*, Multiscale Modeling and Simulation, **8**, (2010), 997-101.

[5] J. Dambrine, *Modélisation et étude numérique de quelques écoulements de fluides complexes en microfluidiques*, Thèse de l'Université Bordeaux 1, (2009).

[6] J. Dambrine, B. Géraud and J.B. Salmon, *Interdiffusion of liquids of different viscosities in a microchannel*, New Journal of Physics, (2009).

[7] J. Fernandez, P. Kurowski, P. Petitjean, E. Meiburg, *Density-driven unstable flows of miscible fluids in a Hele-Shaw cell*, J. Fluid. Mech., **451**, (2002), 239-260.

[8] C.G. Gal, M. Grasselli, *Instability of two-phase flows: A lower bound on the dimension of the global attractor of the Cahn-Hilliard-Navier-Stokes system.*, Physica D, **7**, (2011), 629-635.

[9] D. Gérard-Varet, N. Masmoudi, *Relevance of the slip condition for fluid flows near an irregular boundary*, Comm. Math. Phys., **295**, (2010), 99-137.

[10] A. Günther, K.-F. Jensen, *Multiphase microfluidics: from flow characteristics to chemical and material synthesis*, Lab on a Chip, (2006)

[11] D. Joseph and Y. Renardy, *Fundamentals of two fluid dynamics*, Springer (1993).

[12] G. Karniadakis and A. Beskok, *Micro Flows: fundamental and simulation*, Springer-Verlag, (2002).

[13] O. Kuksenok and A.C. Balazs, *Simulating the dynamic behavior of immiscible binary fluids in three-dimensional chemically patterned microchannels*, Physical Review E, (2003)

[14] O. Kuksenok and A.C. Balazs, *Structures formation in binary fluids driven through patterned microchannels: effect of hydrodynamics and arrangement of surface patterns*, Physica D, (2004).

[15] S. Li, J. Lowengrub, P. Leo, *A rescaling scheme with application to the long-time simulation of viscous fingering in a Hele-Shaw cell*, J. Comp. Phys., **225**, (2007), 534-567.

[16] X.-D. Liu, S. Osher and T. Chan, *Weighted Essentially Non-Oscillatory schemes*, Journal of Computational Physics, **115**, (1994), 200-212.

[17] N.-T. Nguyen, Z. Wu, *Micromixers - a review*, Journal of Micromechanics and Microengineering, (2010).

[18] P.G. Saffman and G. Taylor, *The penetration of a fluid into a porous medium or Hele-Shaw cell containing a more viscous liquid*, Proc. of the Roy. Soc. London Ser A, **245**, (1958), 312-329.

[19] D. Schafroth, N. Goyal and E. Meiburg, *Miscible displacements in Hele–Shaw cells: Non-monotonic viscosity profiles*, European Journal of Mechanics B/Fluids, **3**, (2007), 444-453.

[20] J. Simon, *Compacts sets in the Space $L^p(0,T;B)$.*, Annali. Mat. Pura. Applicata., **4**, (1987), 65-96.

[21] A.D. Stroock, S.K.W. Dertinger, A. Adjari, I. Mezić, H.A. Stone and G.M. Whitesides, *Chaotic mixers in microchannels*, Science, (2002).

[22] A.D. Stroock, S.K.W. Dertinger, G.M. Whitesides and A. Adjari, *Patterning flows using grooved surfaces*, Analytical Chemistry, (2002).

E-mail address: mcolin@math.u-bordeaux1.fr
E-mail address: colin@math.u-bordeaux1.fr
E-mail address: julien.dambrine@math.univ-poitiers.fr